ARTICLE

JOURNAL`S UNIVERSITY OF BABYLON FOR ENGINEERING SCIENCES (JUBES)

مـــجلـة جـــامعة بـــابـل للعلـــوم الهندسية

Vol. 34, No. 1. \ 2026 ISSN: 2616 - 9916

A Numerical Investigation of Composite Beams Incorporating Rectangular and Circular Web Openings with Multiple Shear Connector Types

Ali Habeeb Noori*[1], Abdulnasser Mohammed Al-Jafar'[1]

1 Department of Civil Engineering, College of Engineering, University of Basra, Basra, Iraq

Correspondence * Ali Habeeb Noori Basra, Iraq Email: pgs.ali.habeeb@uobasrah.edu.iq

Received:	2/11/2025	Accepted:	9/2/2026	Published:	31/3/2026

Abstract

The present research provides a numerical evaluation of composite beams with openings constructed with various shear connections under four-point loading conditions. A series of composite steel-concrete beams with varying opening shapes, numbers of openings, and various types of shear connectors have been analyzed numerically. Four variables were examined: connection ratios of 100%, 70%, and 50%; types of shear connectors (studs and Y-rib connectors); shapes of web openings (rectangular and circular); and the number of openings. The conclusion of the research includes the mid-span beam deflection, cracking load, crack pattern, and failure mode. These results indicate that the Y-rib shear connections performed better than all other connectors. They enhanced the ultimate shear capacity by roughly 1.88%, 2.28%, and 3.21% for connection ratios of 50%, 70%, and 100%, respectively. Further, the incorporation of web openings reduces the stiffness and strength of composite steel-concrete beams while increasing their load-bearing capacity and deformation capability. Web opening influences the composite steel-concrete beams and reduces the stiffness and strength of simply supported composite steel-concrete beams. On the other hand, it has been demonstrated that circular web openings perform effectively in all aspects, including keeping stress low at the web openings and simplifying construction. Nevertheless, shear failure was the most common kind of failure in all composite beam samples.

Keywords:- Composite beams, Circle opening, Y-rib connector, Failure mode, Structural behaviour.

I. Introduction

Engineers consistently aim to enhance the materials and processes of design and construction. One of these improvements, a development in built-up structural components, appeared in the early 1900s in the United States, the United Kingdom, and Germany, resulting in the creation of composite construction techniques. Composite steel-concrete beams provide a combination of durability, strength, flexibility in design, toughness, and cost-effectiveness, giving composite structures an attractive option for several major building projects. Furthermore,

Composite Steel-Concrete Beams assist in the decrease, as well as the elimination, of formwork and shoring, thus improving the dimensional stability of structural elements and reduce the consumption of structural steel. [1-2].

Steel-concrete composite structures consist of cross-sections created by reinforced concrete and steel profiles, which combine to resist the applied stresses. The main advantage of composite beams is the combined interaction between concrete and steel: concrete mainly resists compression, whereas steel resists tension. This leads to a reduction in steel usage and the activation of an efficient width of the concrete slab that will enhance the structure strength. In multi-story structures using composite beams, the concrete slab, referred to as the conventional floor, is positioned on the upper flange of the steel profile. A composite beam is commonly found in modern buildings, where steel beams are affixed to the concrete slab by multiple shear connections, helping them to operate as a single unit [3]. Shear connectors are generally connected between the steel beam and concrete slab to prevent longitudinal sliding and vertical separation (pull-out) between the concrete slab and steel girder. During the early 20th century, researchers have utilized mechanical shear connectors to produce shear connections for steel-concrete beams. Headed stud stud connectors are widely used in composite beams due to their performance characteristics. The behaviour of the shear connectors is classified according to the capacity resistant to the shear flow that occurs at the steel-concrete interface and the relationship between force and slip, whether flexible or rigid. A flexible connector approaching its ultimate strength continues to bend without failure, enabling neighbouring connectors to increasingly accept the shear flow. The flexible characteristics of headed stud connections, which permit slippage between the concrete slab and the steel profile even before obtaining the ultimate limit state, substantially contribute to the common application of this connector type [2]. In contrast to the flexible connector, the rigid connector lacks the capacity to deform after the maximum force is exceeded. The resistance to shear stress and the stiffness of the steel-concrete connection are dependent, not only on the shear connector's resistance, but also on the concrete slab's capacity to resist the cracking caused by the high shear stress concentration at each connector [4-5]. Consequently, composite beams are usually produced by partial contact. This means that the shear connectors' combined strength is lower than the steel profile's tensile strength or the lowest compressive strength of concrete.

Overall, extensive studies [6-10] as well as well-developed design procedures have made these connections more prevalent in the construction industry. Marshall et al. [11] performed several studies on reinforced composite beams, including push-out tests using high-strength bolts instead of welded studs. Kwon et al. [12-13] investigated a study utilizing certain high-strength bolts as shear connectors. The study showed that all three varieties of high-strength bolts exhibited enhanced fatigue characteristics compared to the welded shear studs commonly utilized in practice. Moynihan and Allwood [14] assessed three composite concrete specimens of varying lengths (2, 5, and 10 m), constructed with M20 bolts as removable shear connectors. The

results indicated that reinforced composite beams using bolted connections had equivalent moment capability to composite beams with welded shear studs. Mirza et al. [15] conducted experimental push-test investigations with blind bolts. Research results demonstrate that these bolted connections display performance comparable to that of welded headed shear connectors.

Web openings assist the passage of utilities through beams, hence reducing story height. A reduction in building height reduces both the external surface area and the internal volume, thereby decreasing operational and maintenance costs. Conversely, the study of composite concrete beams with web opening has received significant interest from researchers, resulting in major developments in the field of welded studs attached to composite beams, including web openings. Recent experimental and theoretical investigations have been conducted on composite steel-concrete beams, including rectangular, triangular, or circular web openings arranged in a discontinuous series across the beam [16-18]. Early studies were significant for creating models to calculate resistance in the building of composite beams that have rectangular openings. Therefore, Granade's study [19] is significant for presenting tests aimed at predicting stresses according to the Vierendeel mechanism theory. The theoretical stress estimations were found to be incorrect when compared to experimental tests. Granade's work [19] was essential to the advancement of the analytical model by Todd and Cooper [20]. The authors defined that the presence of the rectangular web opening significantly decreases the strength of composite beams; within the area of the opening, the compression strains in the concrete remain not significant, even after the steel yielding.

The structural behavior of the reinforcing composite specimens with openings for the test was simulated using three-dimensional finite element modeling. The concrete's behavior was simulated by defining damage criteria with the concrete damage plasticity (CDP) module in ABAQUS finite element software. Over the last thirty years, researchers have performed numerous experimental and theoretical investigations on the structural behavior of composite beams with web openings [21–33]. In 1968, Granade (referred to in Clawson and Darwin, 1980) conducted the first experiments on composite beams containing rectangular web openings [34]. Granade performed two experiments utilizing rectangular openings with heights and depths corresponding to 60 and 90 percent of the steel section depth, respectively. Both tests were performed on a singular beam with a solid slab. Granade aimed to predict the experimental stresses using Vierendeel analogy. In his analysis, he proposed that the points of contra-flexure in the tees be located along the opening centerline. The predicted stresses were inaccurate. Liao et al. [35] conducted a nonlinear study of reinforced concrete composite beams with rectangular web openings using ANSYS software. Li et al. [36] reported the experimental results of six continuous composite beams containing rectangular web openings. Nevertheless, the majority of the current research was based on cast-in-situ steel-concrete beams utilizing normally welded shear studs as shear connections. Clawson et al. [21] conducted bending experiments on six composite concrete specimens, including rectangular web openings and one steel beam, to study

moment-to-shear ratios ranging from 0.9 to 10 m. The failure mechanism of the specimens tested with lower moment-shear ratios involved the formation of plastic hinges in the metal web opening and diagonal tension failure of the concrete block. Redwood et al. [23] examined the importance of shear connections concerning the dimensions of web openings and the effects of unshored structures. The study's results demonstrated that a high shear-to-moment ratio during loading significantly affected the load-carrying capacity due to a minimal shear connection in the web opening length. Park et al. [26] noted that the failure mechanism of the concrete block depends on the thickness of the slab. The concrete specimens subjected to composite testing with a large slab showed pullout failure at the shear connections, whereas those with a narrow slab width encountered diagonal tension failure in the concrete block. Ellobody et al. [37] performed finite element analysis on composite samples that included stiffened and unstiffened web holes. The research indicated that composite beams with horizontal stiffeners had superior load-bearing capacity compared to those with unstiffened web holes. The research findings suggest that bolted shear-connected composite beams, including web openings, may exhibit comparable mechanical properties.

Hu et al. [38] examined five full-scale composite beams including reinforced web holes that were fabricated and tested using three-point bending, to evaluate the influence of type of stiffener and cross-sectional dimension on the flexural strength of composite beams. The study found that adding longitudinal stiffeners to web openings greatly improved the strength of the composite beams. Mastan et al. [39] planned to enhance the shape and positioning of the aperture to augment its structural efficacy. Three shapes (circle, rectangle, and triangle) were examined in the composite steel-concrete beam and studied utilizing ABAQUS v6.14. Web openings influence the load-bearing and deformation capacities, while reducing stiffness and strength of composite steel-concrete beams. The maximum stress zone of the steel beam rose by 25%, 67%, and 72% for beams with circular, rectangular, and triangular perforations, respectively, compared to the beam without an opening. The reported reductions in stiffness are 7%, 19%, and 12.74% for SCCB with rectangular, circular, and triangular apertures, respectively, as compared to CSCB without a web hole. A deflection increase of 14%, 33%, and 47% has been observed for the circular, rectangular, and triangular opening composite beams, respectively, compared to the beam without openings. Circular web openings have demonstrated significant advantages, including less stress concentration at the openings and increased manufacturing efficiency.

Previous research indicates that there are limited numerical studies about the structural behavior of composite steel-concrete beams incorporating web holes. Thus, more numerical analyses are necessary in this field. This study develops and analyzes a computational model for composite beams containing web openings subjected to shear failure mode. The primary parameters in this study are the configuration of the openings, the number of openings, the types of shear connectors, and the connection ratio of shear connectors. Two varieties of shear

connectors, namely bolt studs and Y-shaped connectors, were utilized. The finite element models have been validated by comparing the load-deflection response outcomes from previous experimental and simulated studies. Three-dimensional non-linear finite element models were developed using ABAQUS to simulate the analyzed composite beams. The interface slip between the concrete block and the I-steel beam of the tested composite specimens was studied using finite element techniques (FEM). The failure modes, ultimate failure load, crack patterns in concrete slabs, ultimate shear capacity, cracking load, load-deflection, strain in compression concrete were examined.

II. Previous Experimental Work

This research involves a numerical assessment that compares the test results of prior research by Li et al. [40] with the finite element analysis results of the current study. Li et al. [40] cast and tested six reinforced concrete composite beams under static loads until failure. The tested composite beams were made from a hot-rolled steel section from China that is HM250 × 125 × 6 × 9 mm. All tested composite beam specimens had concrete slabs with a thickness of 100 mm, a width of 600 mm, and a length of 2350 mm (see Figure 1). All samples were constructed with rectangular web openings sized 300 mm in width and 150 mm in depth. The measurements of the web hole are primarily established for enabling the passage of many pipes, which include those for water, electricity, heating, and communication. The utilized high-strength bolts were all grade 10.9, M16 × 120 mm hexagonal high-tension friction-grip bolts. Figure 1 illustrates the longitudinal viewpoint of the evaluated composite beams. The bolt holes of the composite beam specimens were pre-drilled. Figure 2 provides additional information regarding the schematic configuration. The average compressive strength (fc') of the concrete used in the slab specimens is 30 MPa. Figure 3 exhibits the longitudinal image of the evaluated composite beams, while Table 1 delineates the parameters of the tested beams. A universal testing machine applied a static load to all reinforced concrete beams until failure occurred. The experiment was performed on a 50-ton load testing apparatus under a monotonic, concentrated pressure. Figure 3 illustrates the configuration of the composite beams subjected to a three-point load test. The standard testing methodologies provided in the Standard for Test Method of Concrete Structures (Chinese Code GB/T50152-2012) were employed. Figure 4 shows the whole measuring apparatus, wherein the specimen underwent two cycles of loading and unloading to avert relaxation in the components of the loading mechanism, followed by reloading up to failure.

ARTICLE
JOURNAL`S UNIVERSITY OF BABYLON FOR ENGINEERING SCIENCES (JUBES)
مـــجلـة جـــامعة بـــابـل للعلـــوم الهندسية
Vol. 34, No. 1. \ 2026 ISSN: 2616 - 9916

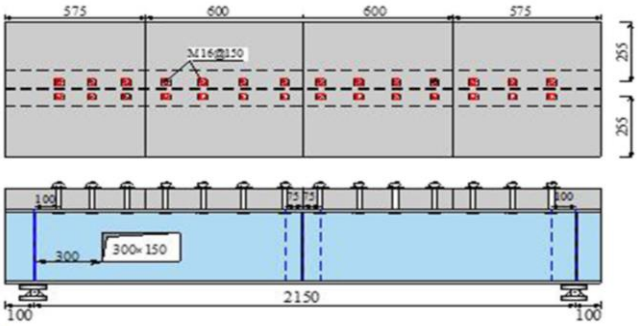

Fig. 1: Composite beam details, (all dimensions are in mm) [40].

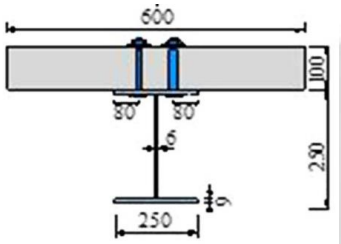

Fig. 2: Typical cross-section of steel beams HM250x125x9x6 [40].

Fig. 3: The 50-ton hydraulic testing machine [40].

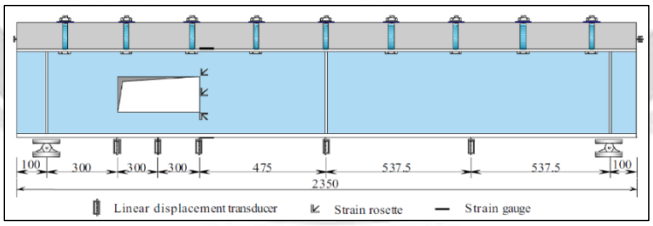

Fig. 4: Setup of test measurements [40].

Table 1. Properties of the tested composite beams.

Beam Designation	Connection Ratio	Number of Openings	Shape of Openings	Location of openings	Type of connector	Stud spacing
C50	50%	0	…….	……	Stud	7@342
C70	70%	0	……	……	Stud	10@222
C100	100%	0	…..	……	Stud	14@150
C50R	50%	1	Rectangular	Center	Stud	7@342
C70R	75%	1	Rectangular	Center	Stud	10@222
C100R	100%	1	Rectangular	Center	Stud	14@150
C50R2	50%	2	Rectangular	Center	Stud	7@342
C70R2	70%	2	Rectangular	Center	Stud	10@222
C100R2	100%	2	Rectangular	Center	Stud	14@150
C50R3	50%	3	Rectangular	Center	Stud	7@342
C70R3	70%	3	Rectangular	Center	Stud	10@222
C100R3	100%	3	Rectangular	Center	Stud	14@150
C50C	50%	1	Circle	Center	Stud	7@342
C70C	70%	1	Circle	Center	Stud	10@222
C100C	100%	1	Circle	Center	Stud	14@150
C50Y	50%	0	……	……	Y-Rib	7@342
C75Y	75%	0	…….	……	Y-Rib	10@222
C100Y	100%	0	……	……	Y-Rib	14@150
C50RY	50%	1	Rectangular	Center	Y-Rib	7@342
C70RY	75%	1	Rectangular	Center	Y-Rib	10@222
C100RY	100%	1	Rectangular	Center	Y-Rib	14@150
C50R2Y	50%	2	Rectangular	Center	Y-Rib	7@342
C70R2Y	70%	2	Rectangular	Center	Y-Rib	10@222
C100R2Y	100%	2	Rectangular	Center	Y-Rib	14@150
C50R3Y	50%	3	Rectangular	Center	Y-Rib	7@342
C70R3Y	70%	3	Rectangular	Center	Y-Rib	10@222
C100R3Y	100%	3	Rectangular	Center	Y-Rib	14@150
C50CY	50%	1	Circle	Center	Y-Rib	7@342
C70CY	70%	1	Circle	Center	Y-Rib	10@222
C100CY	100%	1	Circle	Center	Y-Rib	14@150

III. Finite Element Analysis Using Abaqus

A. Geometrical modelling

Each specimen consisted of four parts: a concrete slab, a steel beam, a lateral stiffener, and shear connectors. The concrete slab, flange, web, and lateral stiffener were simulated utilizing 3D models and reliable shell planers for these parts. However, solid elements in ABAQUS can experience both linear and complicated nonlinear analyses, incorporating contact, plasticity, and significant deformation [41-44]. In the recent work, the first-order reduced

integrated 3D component (C3D8-Brick) is used to design for the concrete slab, load-bearing plates, and end plates present in Figure 5 [45]. On the other hand, the reinforced steel bars and shear connectors were modeled using a 2-node linear 3-D truss element known as T3D2, which is available in ABAQUS [45, 46]; see Figure 6. Table 2 shows the two elements used in the present numerical model. Nevertheless, as seen in Figure 7a, shell components were used to present structures characterized by having one dimension where the thickness is considerably smaller than the other dimensions. The thickness is determined by the sectional property, which indicates each component independently in a three-dimensional shell plane corresponding to its dimensions. Full 3-D elements are provided in this model, and element thickness is determined by section characteristics, the values of which are displayed in Table 2. ABAQUS assigns only specific section characteristics utilizing this thickness. Numerous different elements dealing with both non-homogeneous and homogeneous materials have been created by ABAQUS. The thin steel panels are shown in Figure 7b [47], which is a three-dimensional model made up of rectangular S4R shell elements or triangle elements at six degrees of freedom in each node.

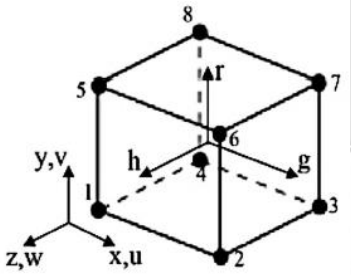

Fig. 5: (C3D8) in ABAQUS [45].

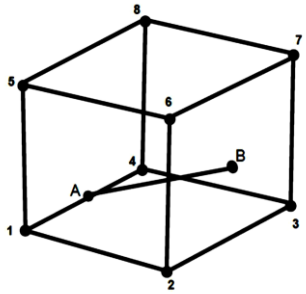

Fig. 6: 2-Node 3-Dimension Truss Element [45, 46]

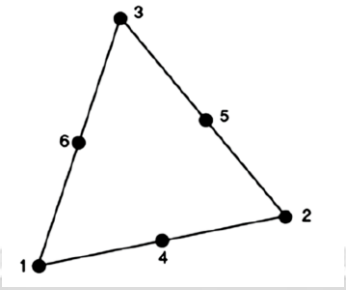

a-Triangular elements

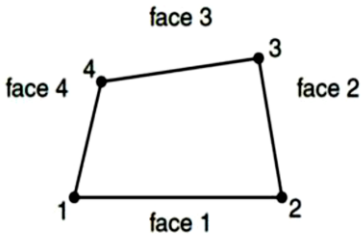

b- Rectangular elements

Fig. 7: Node shell element [47]

Table 2. Summary of all types of elements used in the numerical model.

Element	Element type
Concrete slab	C3D8R
Reinforcing steel	T3D2
Flange	Shell: planar
Flat web	Shell: planar
Stiffener	Shell: planar
Shear connector	T3D2

B. Material modelling

a. Plasticity parameters

The concrete damage plasticity (CDP) model used by ABAQUS/Standard simulates the behavior of conventional concrete until failure. Concrete is typically characterized as a homogenous building material. In the present model, numerous significant plasticity parameters for the RC slab were maintained at ABAQUS's default configurations. The CDP model needs a description of the following elastic and plastic characteristics of the concrete [48]. Nevertheless, the CDP includes multiple factors, some of which are obtained from experimental testing. In the present model, several essential plasticity parameters for the reinforced concrete slab remain at ABAQUS's default values. Poisson's ratio and the material's modulus of elasticity have been utilized to prepare for the elastic stage. Conversely, ABAQUS provides a vast array of models for the plasticity phase based on the material's behavior following the elastic phase. Malm [49]

proposes that there is higher consistency with the experimental results for dilation angles ranging from 30 to 40 degrees. For standard concrete, a ψ value of 30 is considered suitable. The major CDP parameter values, particularly the dilation angle (ψ) and viscosity (μ), were established according to previous guidelines [50-51] and calibrated with the study's data. Table 3 and 4 illustrate the probable elastic and plastic properties of the engineered concrete components in ABAQUS.

Table 3: Elastic values for the current simulations model.

Parameters	Assumed value
Elastic modulus E	36539
Poisson's ratio ν	0.2

Table 4: Plastic values for the current simulation model.

Parameters	Assumed value
K	0.667
Potential eccentricity ε	0.1
Dilation angle Ψ	51
fb_0/fc_0	1.16

b. Compressive behavior of concrete

In compression, concrete was simulated using a parabolic shape (Figure 8). The predicted relationship of concrete stress-strain under uniaxial compressive force may be divided into three phases. The first section exhibits a linear-elastic range, defined by an initial elastic modulus, E. The linear range of stresses stops at the stress level ($\sigma c_{\circ}$), which is defined here as two-thirds of fc. The second section demonstrates the upward portion of the uniaxial stress-strain relationship, corresponding to the application of compression until the maximum load is reached at the specified strain level. The secant elastic modulus is denoted as Esec. The third phase of the stress-strain response, following the peak stress and preceding the ultimate strain εu, refers to the post-peak range.

Figure 9 illustrates a typical stress-strain relationship of uniaxial concrete compressive strength in the finite element model. To provide the required data for the CDP model in compression, the experimental stress-strain curves must be converted to stress-inelastic strain relations. The inelastic strain could be determined using equation 3.1:

$$\varepsilon_c^{in} = \varepsilon_c - \varepsilon_c^{el} \quad (1)$$

Where: $\varepsilon_c^{el} = \frac{\sigma_c}{E_0}$

ε_c^{in}: inelastic strain

ε_c: total strain

ε_c^{el}: elastic strain

σ_c: concrete strain

E_0: elastic modulus of elasticity

Figure 10 presents data designed for use in ABAQUS software for Normal Concrete (NC) under compression.

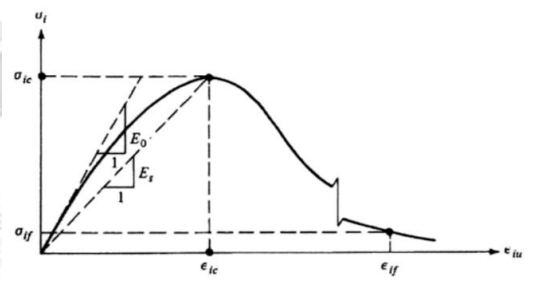

Fig. 8: Concrete behavior to uniaxial strain as indicated in the ABAQUS theory manual [52].

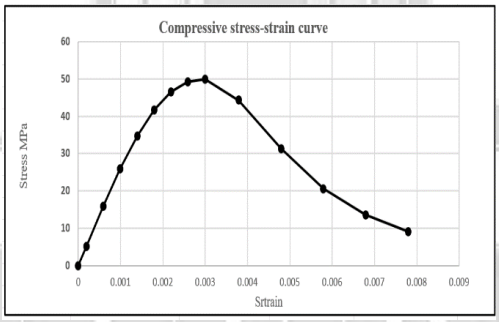

Fig. 9: Normal compressive stress - inelastic strain relation.

c. Tensile behavior of concrete

ABAQUS offers three different methodologies for defining tension-softening behaviour: stress-strain relation, stress-displacement relation, or the application of fracture energy (Gf) [53]. The current study investigates the stress-strain relationship of normal concrete under tension, which was modelled using the relationship proposed by Massicotte et al. [54], as shown in Figure 10. The stress-strain curves in tension have been converted into stress-inelastic strain relationships, as seen in Figure 11 for normal concrete, similar to the compression behaviour. The stress-strain relationship in concrete subjected to uniaxial tension stress is linear elastic before the stress exceeds the ultimate tensile stress; after that, micro-cracks form with a tension-softening response.

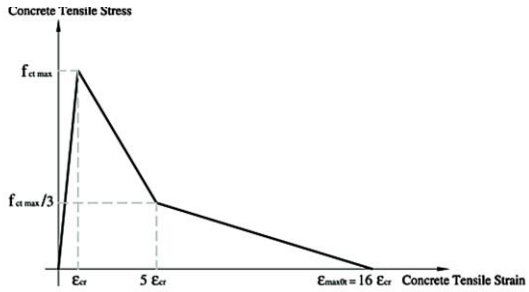

Fig. 10: Tension-softening curve proposed by Massicotte et al. [48].

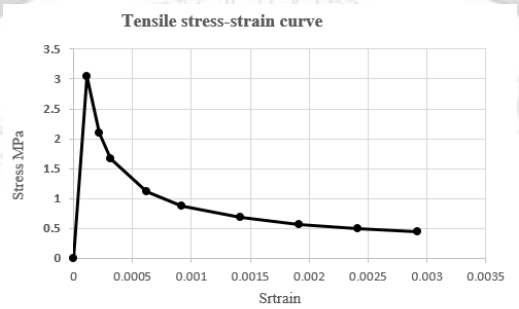

Fig. 11: Normal tensile stress -strain relation.

For the reinforcement bars, Young's modulus E and Poisson's ratio υ, reflect the stress-strain relationship as shown in Figure 12, Where E is typically around 200,000 MPa and υ is around 0.3. Table 5 displays the plastic properties, such as the yield stress and the associated plastic strain. The stress-strain curves for steel considered in this simulation are shown in Figure 12.

Table 5. Characteristics of the steel bar.

Bar Diameter, mm	Elastic properties		Plastic properties	
	Modulus of elasticity (E)	Poisson's ratio (υ)	Yield stress (MPa)	Plastic strain
Ø8	200000	0.3	298.39	0.006

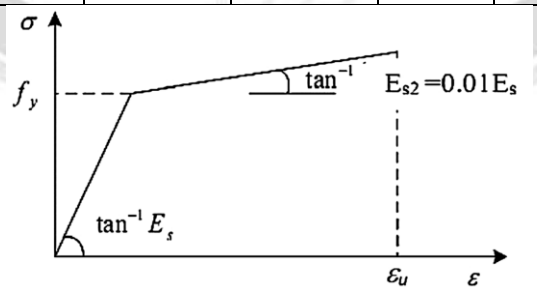

Fig. 12: Stress-stain curve for steel [46].

d. Modeling of steel girder

Steel can be characterized as a homogeneous material, demonstrating identical stress-strain behavior under both tensile and compressive forces within a specific range. The computer models mainly depend on the input of appropriate parameters to produce accurate and effective results. The material properties have been verified by tensile test samples, as described in previous research by Li et al. [40]. The characteristics are utilized in complete steel girder models, and the chosen element requires the parameters for both linear and nonlinear behavior. The specified element may produce a uniform relationship between strain and stress on both the tensile and compressive sides [46]. Figure 13 illustrates the empirical stress-strain curve for steel.

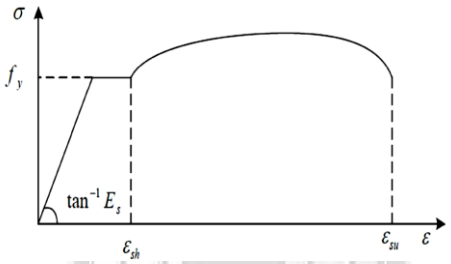

Fig. 13: Curve of stress-strain for steel material [52]

The relationship between strain and stress can be split into two elements: the initial component has a slope equal to Es, while the second part is designed to exhibit a zero slope; however, for computational analysis, an amount of 0.01Es is employed, as illustrated in Figure 5.3 [47]. Table 6 presents an overview of the properties employed in the finite element analysis of ABAQUS.

Table 6: Characteristics of the steel girder

Elastic stage		Plastic stage				
Modulus of elasticity (E)	Poisson's ratio (υ)	Stress, MPa			Plastic strain	
200000	0.3	Flange	f_y	225	ε_e	0
			f_u	390	ε_p	$\frac{390-225}{0.01x200000} = 0.0825$
		Web	f_y	235	ε_e	0
			f_u	400	ε_p	$\frac{390-225}{0.01x200000} = 0.0825$
		Stiffener	f_y	235	ε_e	0
			f_u	400	ε_p	$\frac{390-225}{0.01x200000} = 0.0825$
		Bolted shear connector (M16)	f_y	932.43	ε_e	0
			f_u	1040	ε_p	0.0825
		Y-rib shear connector	f_y	932.43	ε_e	0
			f_u	1040	ε_p	0.0825

e. Modeling of steel loading plate and supporting plate

The required input data for the loading steel plate and supporting plate refers mainly to the elastic stage. The elastic response is characterised by the modulus of elasticity (E) and Poisson's ratio (υ), which have typical values of 200,000 MPa and 0.3, respectively.

Table 7: Characteristics of the steel bar

Bar Diameter, mm	Elastic properties		Plastic properties	
	Modulus of elasticity (E)	*Poisson's ratio (υ)*	*Yield stress (MPa)*	*Plastic strain*
Ø8	200000	0.3	298.39	0.006

C. Assembly of the numerical model

The numerical model of the composite beams consisted of different parts. The components included the concrete slab, steel reinforcement, steel girder, bolt stud connections, Y-rib connections, stiffeners, load, and supporting plate. These parts were created independently, assembled to form the numerical specimen/model. Figure 14 shows the assembly of all components incorporated in the numerical model for this research. Figure 8 shows the assembly of all components incorporated in the numerical model for this research. Stress concentration in the loading and support regions has been reduced by employing steel plates measuring 600 x 150 x 10 mm. The connect form of the CONSTRAIN option in ABAQUS was utilized for connecting these plates to the composite beams. Furthermore, truss elements were utilized in this work to demonstrate the reinforcing bars, which were encased within concrete solid components ("host" continuum) through the creation of embedded region limitations in ABAQUS. Figure 14 depicts the interaction of the steel girder, steel reinforcement, and concrete. The simply supported boundary conditions utilized in the prior experimental test were carried out by modeling the boundary conditions of the beams. After assembly, the components were configured to interact as a composite system.

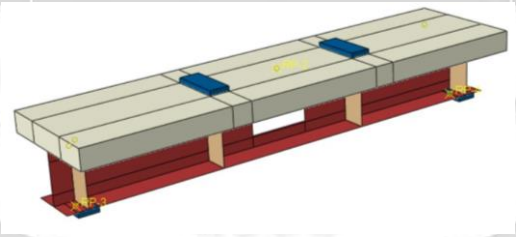

a: Composite beam model in ABAQUS

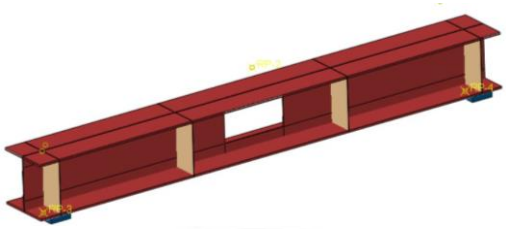

b: 3D View of steel girder

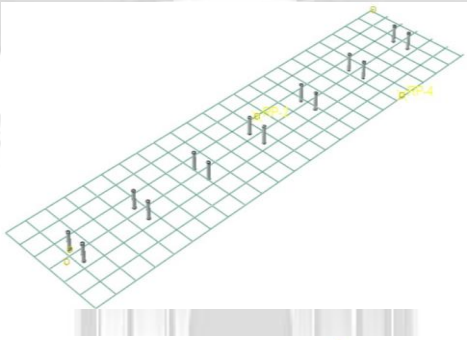

c: 3D View of reinforced concrete slab

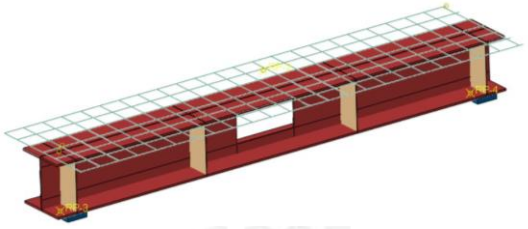

d: 3D View of a composite beam with Reinforcement bar

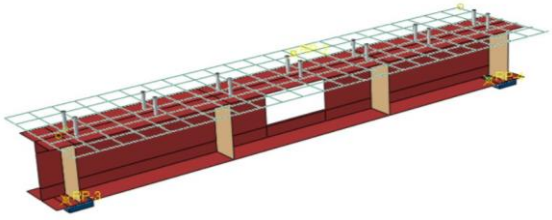

e: 3D View of an composite beam with bolts stud connectors

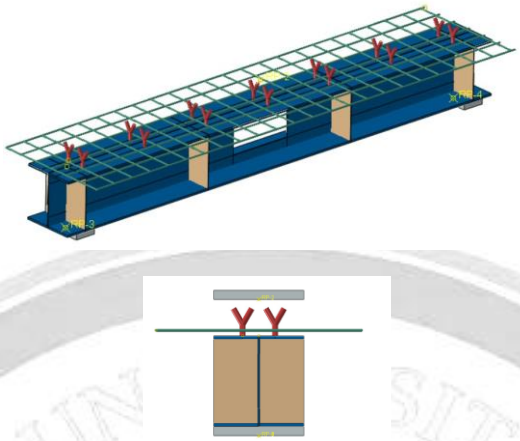

f: 3D View of a composite beam with Y-rib connectors

Fig. 14. Assemblage of the composite beam's numerical models

D. Loading and boundary conditions

The load was generally static, expressed as displacement control representing at mid-span (reference point), and was uniformly distributed throughout the plate surface in each loading zone. For modelling the identical boundary conditions shown in the previous experimental testing, the displacement/rotation mechanism in ABAQUS was utilised to model the simple supports of the composite beam as follows:

Pin supports: The nodes are fixed to the lower middle of the support plate along the transverse axis, resisting translation in all directions of vertical (direction Y), lateral (direction x), and longitudinal (z direction). All axes of the nodes are free to turn.

Roller support: The nodes are affixed to the bottom central portion of the support plate along the transverse axis and are permitted to translate just in one direction (Z direction). All axes of the nodes are free in their rotation. Figure 15 illustrates the support and loading conditions.

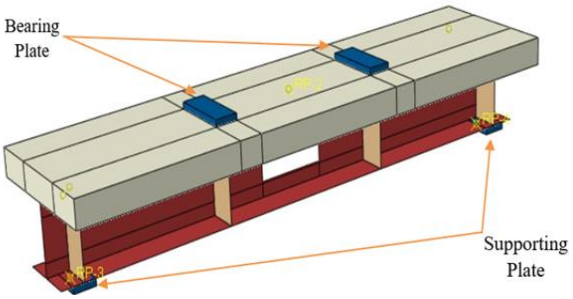

Fig. 15: Loading and boundary conditions used in the current mode.

E. Modeling of Interaction

ABAQUS provides numerous methods for modelling interactions between model members. These installations allow model proximity to accurately simulate the experimental behavior of the test beam specimens observed from the previous experimental work studied by Li et al. [40].

a. Interaction between reinforced bars and the concrete surrounding

The truss elements in this study represented the reinforcing bars, which were confined inside the concrete solid parts ("host" continuum) by the application of embedded region constraints in ABAQUS, as detailed in Figure 16. Embedding allows for the proper connection of each node of the reinforcement element to the nearest concrete node. This bonding type excludes the slip effects of concrete beam reinforcements; nevertheless, this effect has been slightly addressed by the definition of concrete tension softening [53].

Fig. 16: Interaction between steel bars reinforcement and concrete slab.

b. Interaction between steel girder elements

In the steel girder components, steel beams were made as one element in each side (web bound, web top, and flange contact using tie contact types). Figure 17 present the interaction for each side.

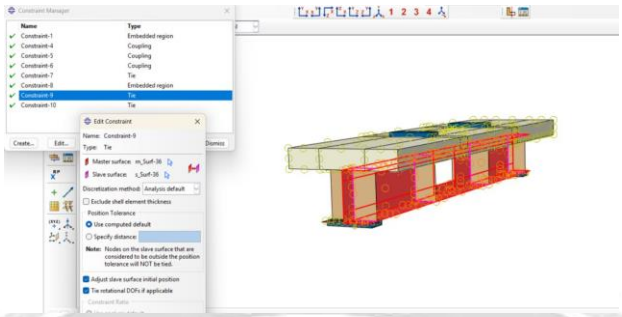

a: Interaction all steel girder beam

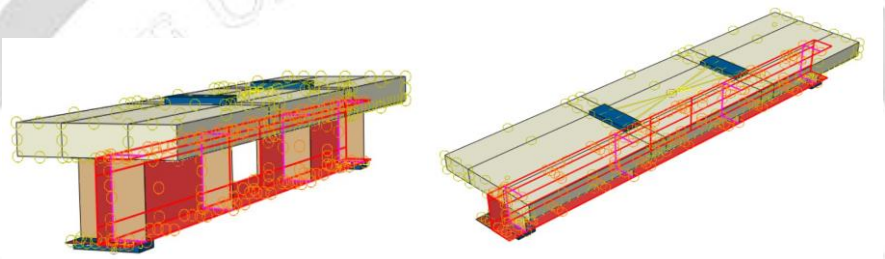

b: Interaction right side of steel girder

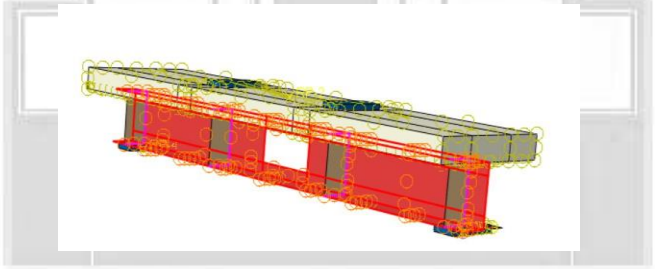

c: Interaction left side of steel girder

Fig.17. Interaction models for steel girder elements.

c. Interaction of beam with the shear connectors

The flange of the steel stud connector and concrete are represented by equivalent rectangular prisms that have a square cross-section to simplify meshing and subdividing the specimens and obtaining hexahedral elements only. The stud connectors offer two types of connections, with the base welded to the top flange of the steel beam, while the external surfaces are surrounded in concrete. The base surface of stud connections is represented in ABAQUS by tie constraints, as has been mentioned and illustrated in Figure 18. The exterior surfaces in contact with concrete are defined by embedded region contact.

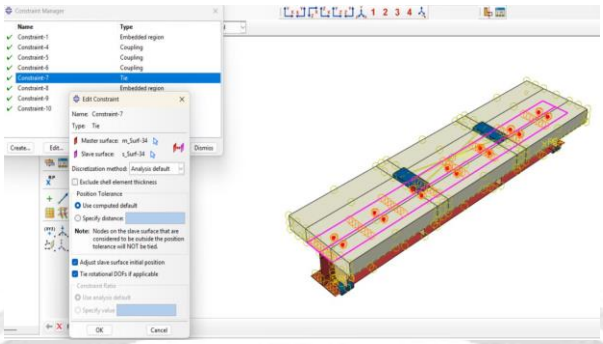

Fig. 18: Define the contact on base.

d. Interaction between steel girder and concrete slab

It was modelled as (master) for the top surface of the steel flange for the beam and modelled as (slave) for the lower surface concrete of the slab. The interaction type is general contact (standard) for modelling samples under load. Figure 19 illustrates the important selection for defining the contact characteristics.

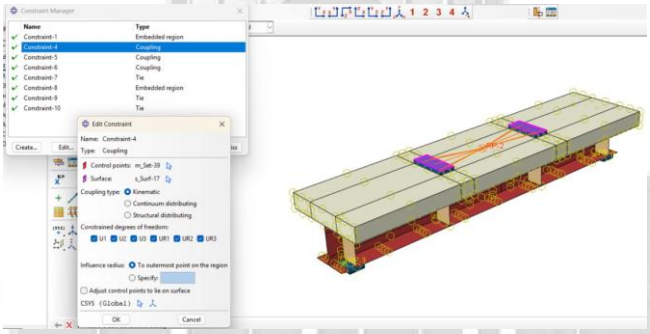

(a) Plate loading

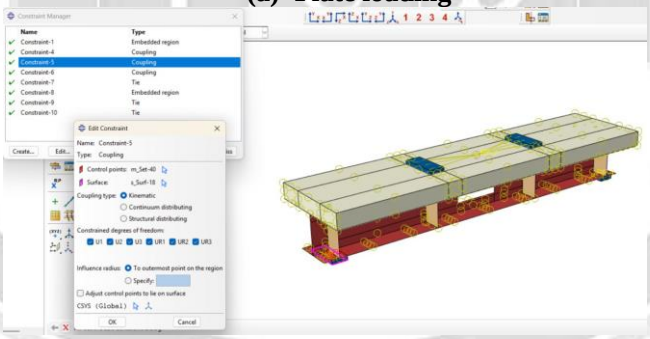

(b) Plate support

Fig. 19: Boundary conditions of composite beam in ABAQUS

e. Interaction of beam with the loading and supporting steel plates

The loading and supporting steel plates are connected to the continuous concrete beam for reducing stress concentrations at the loading and support locations. Constrain general contact standard module prevents

the concrete surface from separating from the plates, indicating that the components cannot be moved during loading.

F. Meshing

To obtain reliable results for the finite element model, each component is carefully adjusted to correspond with the specific mesh size, ensuring that all different materials are connected at common nodes. The preferred mesh form in the model is a hexahedral (brick) structural element. Eight-node brick components with three degrees of freedom (C3D8) per node are employed to simulate the concrete and supporting plates of the mesh. A certain steel bar is designated as a T3D2 truss element. The appropriate mesh size created depends on the aggregate size according to ABAQUS guideline 6.14.

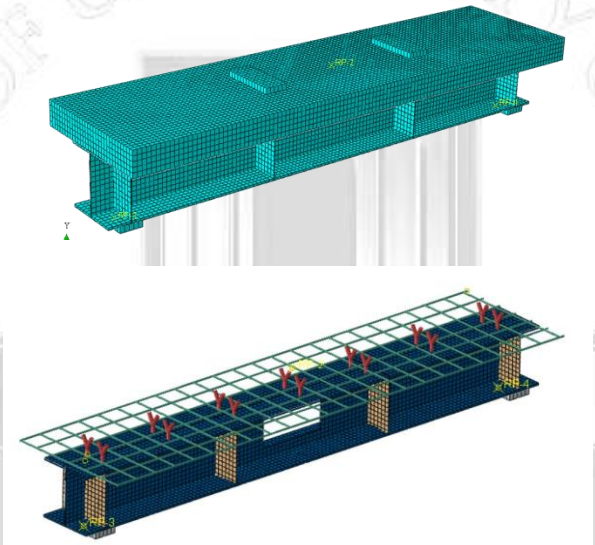

Fig. 20: Finite element meshes for composite beam

IV.Numerical Results And Discussions

Thirty specimens of the composite beam were simulated to investigate their structural behavior. These models are divided into two groups: the first group is a composite beam incorporating stud shear connectors, and the second group incorporates Y-rib shear connectors. Table 8 summarizes the numerical test results for the composite beams, including ultimate capacity, failure load, and failure mode for tested beams with a 50%, 70%, and 100% connector ratio. Eighteen beams contained rectangular web opening with dimensions 300x150 mm. On the other hand, six beams are made with circle web openings. The following sections discuss and evaluate the results along with the load-displacement curves.

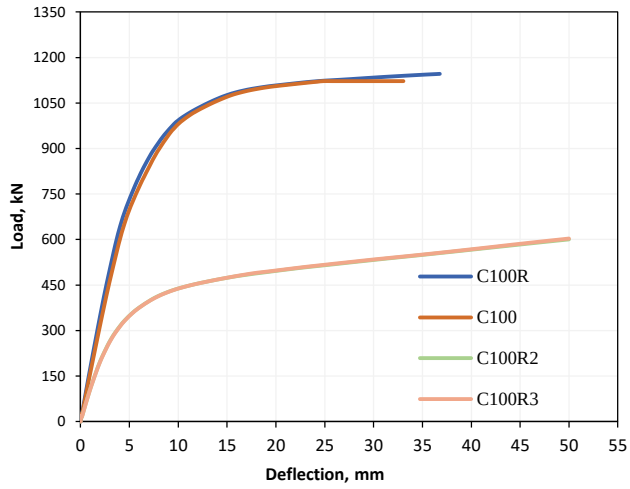

Fig. 21: Load–deflection response for composite beams (studs bolt connections) with and without rectangular web opening.

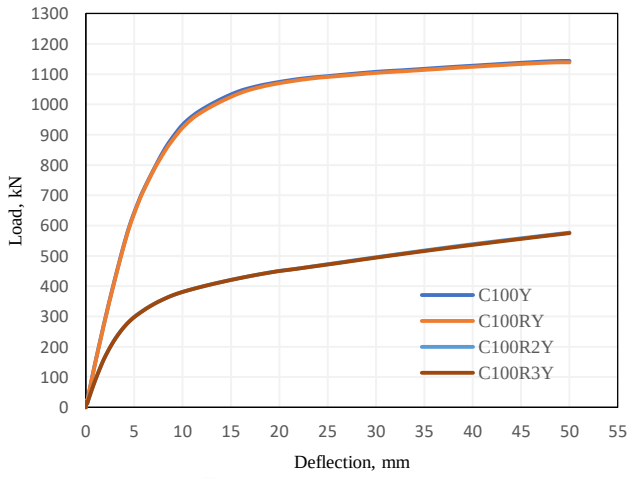

Fig. 22: Load–deflection response for composite beams (Y-rib connections) with and without rectangular web opening.

A. Effect of rectangular web opening

1) Load-mid span deflection response

A rectangular web opening for tested composite beams made with different types of shear connectors (Bolts studs and Y-rib connections) was used to investigate the shear load-deflection responses of the beams, which are depicted in Figure 23-24. Three connection ratios, 50%, 70%, and 100%, were used for each type of connection. For bolt stud connections, three web-opening specimens designated as C-50RS, C-70RS, and C-100RS exhibited a quasilinear response until the peak load. The opening specimens show a slight increase in the maximum failure loads of 2.78%, 1.79%, and 3.43% for C-50RS, C-70RS, and C-100RS, respectively, compared to beams without openings. However, an increase in deflection response of approximately 80.06%, 28.40%, and 16.22%, respectively, when compared to non-opening specimens. Figure 23 shows the shear load-

deflection response of the opening beams with bolt stud connections. The present web opening for composite beams improved the shear response of the non-opening beams. These specimens did not demonstrate a reduction in load or a notable variation in slope at the initiation of shear cracking.

In contrast, opening Y-rib beams reduces the maximum shear strength by about 0.1%, 0.18%, and 0.41% for C-50RY, C-70RY, and C-100RY, respectively, compared to beams without openings. The results also indicated that there were no changes in deflection values at failure loads. Furthermore, the results indicated that there were no corresponding changes in deflection values at failure loads. Additionally, as shown in Figure 24, the stiffness of opening beams is similar to that of reference beams (beams without openings).

Table 8: Summary of the results of the numerical tests

Beam Designation	Number of Openings	Ultimate capacity (kN)	Δ_{max} (mm)	Failure mode
C100	1	1122.07	33.05	Shear Failure
C70	1	1066.62	50	Shear failure
C50	1	1119.02	42.33	Shear failure
C100R	1	1145.98	36.78	Shear Failure
C70R	1	1120.69	33.05	Shear failure
C50R	1	1113.27	44.06	Shear failure
C100R2	2	600.34	50	Shear Failure
C70R2	2	555.308	50	Shear Failure
C50R2	2	525.56	50	Shear Failure
C100R3	3	603.17	50	Shear Failure
C70R3	3	554.698	50	Shear Failure
C50R3	3	525.373	50	Shear Failure
C100C	1	1083.15	50	Shear Failure
C70C	1	1107.98	33.85	Shear Failure
C50C	1	1094.35	45.76	Shear Failure
C100Y	1	1143.58	50	Shear Failure
C70Y	1	1125.99	50	Shear failure
C50Y	1	1103.45	50	Shear failure
C100RY	1	1138.93	50	Shear Failure
C70RY	1	1123.94	50	Shear failure
C50RY	1	1102.94	50	Shear failure
C100R2Y	2	576.78	50	Shear Failure
C70R2Y	2	555.308	50	Shear Failure
C50R2Y	2	525.56	50	Shear Failure
C100R3Y	3	575.06	50	Shear Failure
C70R3Y	3	554.698	50	Shear Failure
C50R3Y	3	525.373	50	Shear Failure
C100CY	1	1107.56	50	Shear Failure
C70CY	1	1096.37	50	Shear Failure
C50CY	1	1080.31	50	Shear Failure

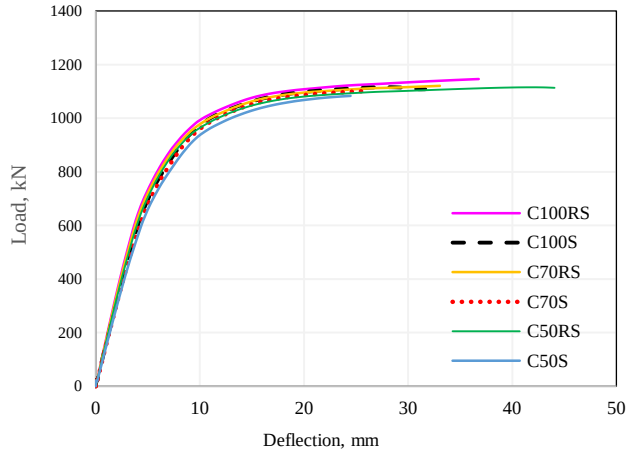

Fig. 23: Load–deflection response for the tested composite beams made with and without rectangular web opening reinforced bolts shear connections.

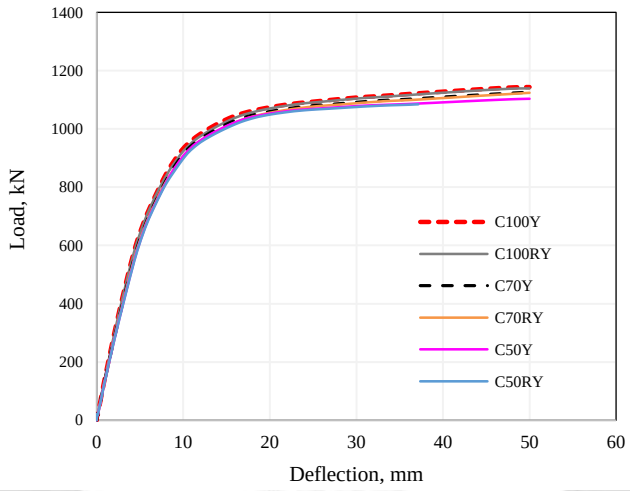

Fig. 24. Load–deflection response for the tested composite beams made with and without rectangular web opening reinforced Y-rib shear connections.

2) Crack Patterns and Failure Modes

Figures 25 and 26 present the crack patterns and failure mode for tested opening composite beams. For all tested opening beams, diagonal cracks initially appeared in the edges of the web openings and extended to the concrete block surrounding the loading site when the load approached approximately 50% of the ultimate load. When the load on samples heightened, the impact of additional bending moments due to

"Vierendeel action" adjacent areas of a web opening, along with the extrusion impacts between proximate concrete panels, became increasingly evident. Shear Failure and crushing concrete in tested specimens was exhibited suddenly upon application of the ultimate failure load. Failure occurs when opening is positioned near the beam's center, where shear is absent, resulting in the yielding of the steel beam above and below the opening and the crushing of the concrete slab.

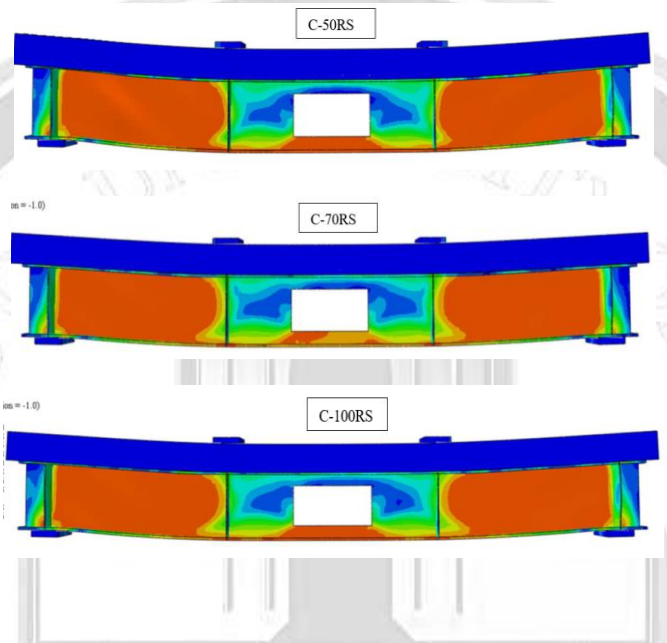

Fig. 25. Crack patterns and mode of failure for opening bolt studs composite beams.

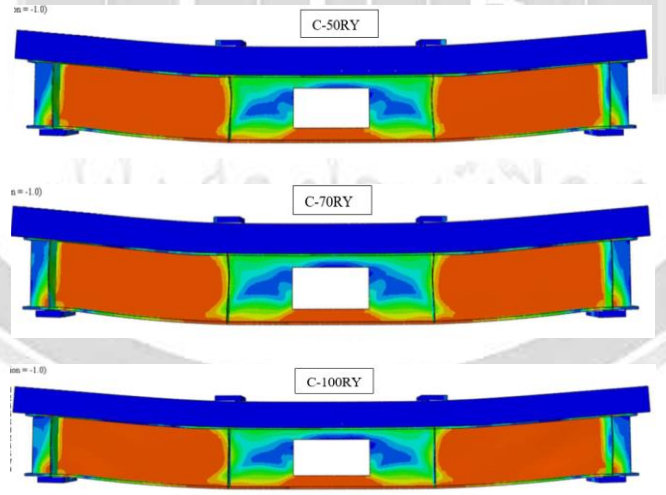

Fig. 26. Crack patterns and mode of failure for opening Y-rib composite beams.

B. Effect of shape opening

1) Load- deflection response

In this group, twelve composite beams were previously mentioned, which were produced with web openings (rectangular and circular web openings). When comparing the numerical results of this group of the opening composite specimens [C100R, C70R, C50R, C100C, C70C, C50C, C100RY, C70RY, C50RY, C100CY, C70CY, and C50CY], which were tested under three-point loading, it can be noted that shear failure occurred for these tested specimens. Table 9 and Figures 27 and 28 present the numerical outcomes of the tested composite specimens. As the shape of the of the web opening changed, the displacements under peak loads of the composite beams made with shear stud connections increased. However, for Y-rib connections, results present that all specimens have the same deflection value. On the other hand, for load-bearing capacity, all the tested specimens present reason load value when using ag a circle opening shape. In the figure, it can be observed that the shear connection specimens with circular and rectangular openings performed similarly of strength, stiffness, and ductility. The same behavior was observed for Y-rib connection beams. The maximum load capacities of the C100R, C70R, C50R, C100RY, C70RY, and C50RY beams are 1145.98 kN, 1120.69 kN, 1113.27 kN, 1138.93 kN, 1123.94 kN, and 1102.37 kN, with corresponding mid-span displacements of 36.77 mm, 33.05 mm, 44.06 mm, 50 mm, 50 mm, and 50 mm (Figure and Table 1). Also, it can be seen that the maximum load capacity of the circle opening specimens is 1083.15 kN, 1107.98 kN, 1094.35 kN, 1107.56 kN, 1096.37 kN, and 1080.31 kN, which is about 3% lower than the reference beams.

Table 9: The ultimate loads and deflection of the tested opening composite beams.

Beam designation	Ultimate capacity (kN)	Failure load increase over Control beam *	Δ_{max} (mm)	Ratio relative to the control beam*	Failure mode
C-100R	1145.98	--	36.77	--	Shear failure
C-100C	1083.15	- 5.48%	50	+35.98%	Shear failure
C-70R	1120.69	--	33.05	--	Shear failure
C-70C	1107.98	- 1.13%	33.85	+2.42%	Shear failure
C-50R	1113.27	--	44.06	--	Shear failure
C-50C	1094.35	-1.69%	45.76	+3.85%	Shear failure
C-100RY	1138.93	--	50	--	Shear failure
C-100CY	1107.56	-2.75%	50	0.00	Shear failure
C-70RY	1123.94	--	50	--	Shear failure
C-70CY	1096.37	-2.45%	50	0.00	Shear failure
C-50RY	1102.37	--	50	--	Shear failure
C-50CY	1080.31	-2.00%	50	0.00	Shear failure

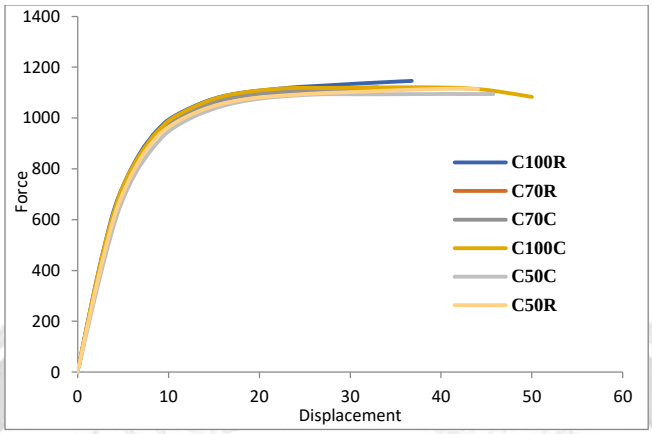

Fig. 27. Load–deflection response for the tested composite beams made with a rectangular and circle web opening reinforced with shear studs connections.

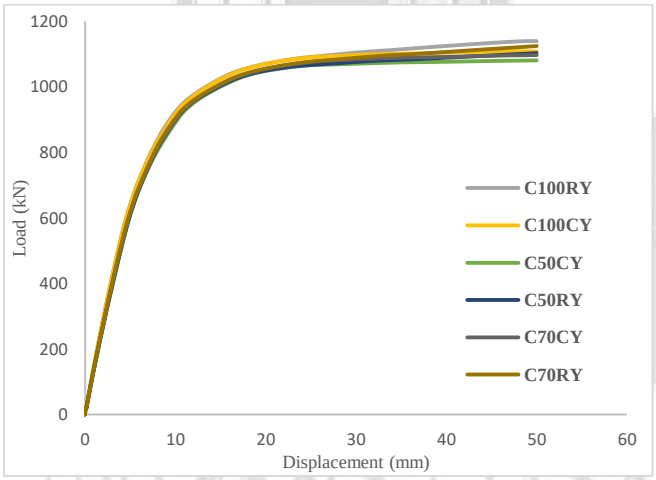

Fig. 28. Load–deflection response for the tested composite beams made with a rectangular and circle web opening reinforced with Y-rib connections.

2) Crack Patterns and Failure Modes

The failure modes of the composite opening beams are illustrated in Figures 29-30. All the tested beams exhibited shear failure loads. From the Figures, it is observed that the shape of openings causes an increase in Von Mises stresses. From the observations, circular web opening has been found to be effective compared to the other openings. For rectangular openings, cracks tend to initiate at the sharp corners of the rectangular openings due to high stress concentration. This led to diagonal shear-tension cracks propagating from the corners downward toward the bottom flange. In cases with insufficient reinforcement or connection

detailing, cracks develop early and extend rapidly. Further, longitudinal cracks may also appear in the concrete slab above the opening, particularly where composite action is weak. On the other hand, in circular openings, crack distribution is more uniform and less severe due to the absence of corners. Radial or curved cracks develop symmetrically around the circular opening. this attributed to the fact that the rounded shape distributes stresses more efficiently, minimizing early crack development. From Figure 29, it was observed that the rectangular opening beams failure is brittle and sudden, dominated by shear failure at opening corners and tensile cracking extending to the flanges resulted to Crushing of the concrete slab above the opening if bond is lost. In contrast, when headed shear studs are used, the risk of premature failure is higher due to limited shear redistribution. For Figure 30, it was found that the circular opening beams were failure tends to be more ductile, with gradual strength degradation. Common failure modes was Web-post buckling and crippling of the web panel. It is interesting to see that the Y-rib connectors improve post-cracking performance and delay failure by better shear distribution.

Table 10: Comparison summary of failure mode for opening composite beams

Feature	Rectangular + Studs	Circular + Studs	Rectangular + Y-Rib	Circular + Y-Rib
Crack Initiation Zone	Sharp corners	Smooth edges	Delayed and controlled	Minimal and delayed
Crack Type	Diagonal (shear–tension)	Radial or curved cracks	Fewer and shorter cracks	Limited radial cracking
Failure Mode	Brittle shear or tearing	Ductile buckling	Controlled yielding	Stable ductile behavior
Failure Location	Corners & bottom flange	Web-post area	Gradual around opening	Localized in web or flange

C100R

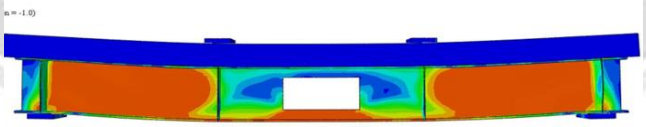

C100C

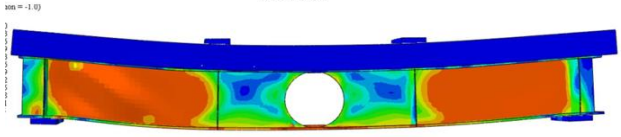

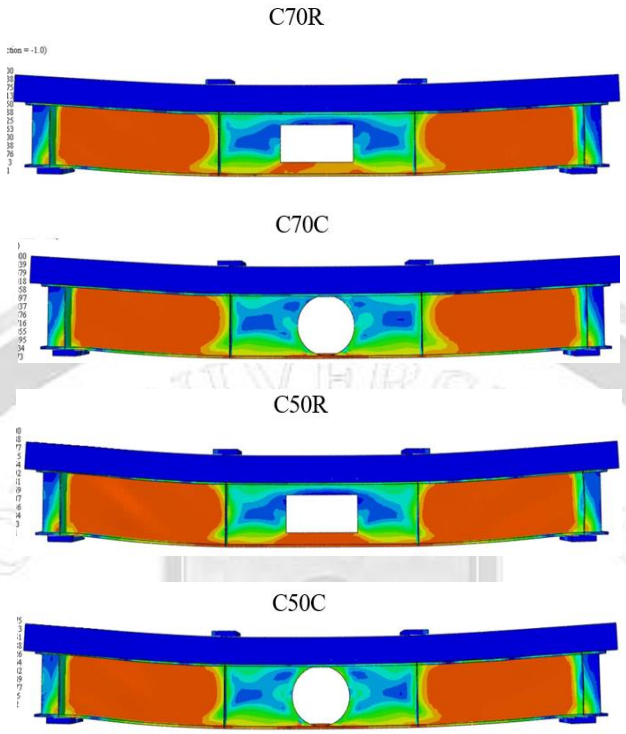

Fig. 29. Crack pattern and failure mode for opening composite beams reinforced shear studs connection.

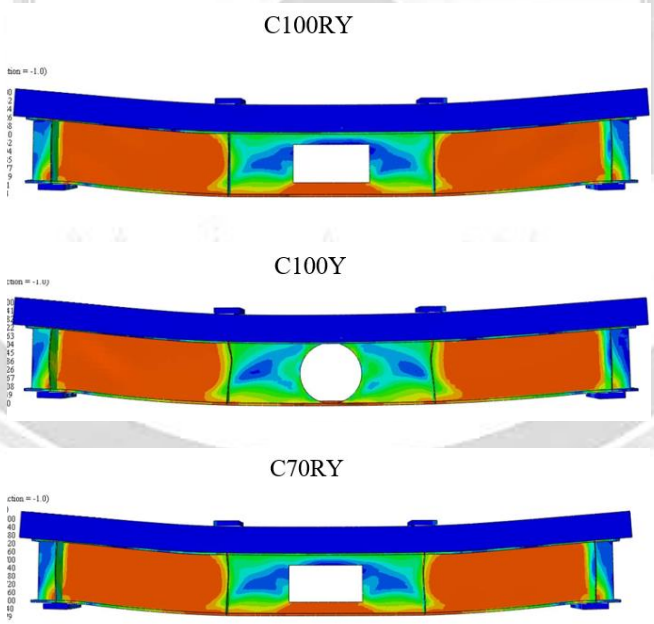

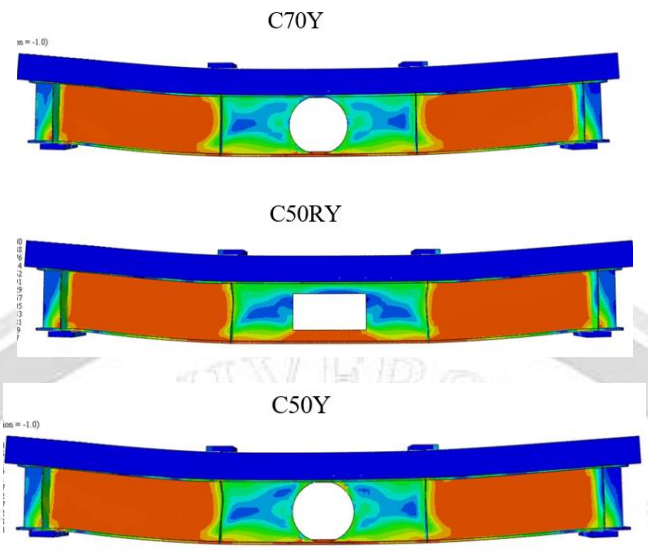

Fig. 30. Crack pattern and failure mode for opening composite beams reinforced Y-rib connection.

C. Effect of number opening

1) Load- deflection response

The influence of web openings on the structural performance of composite beams is a critical factor in design, particularly when service ducts or utility passages require such modifications. In the present study, the effect of introducing one, two, and three rectangular web openings (designated as C-100R, C-100R2, and C-100R3, respectively) was evaluated under shear loading with a 50%, 70%, and 100% connection ratio for shear studs. The load–deflection responses obtained offer useful information regarding the structural implications of increasing the number of openings, as shown in Table 11 and Figures 31-32. The initial stiffness of the beam was observed to decrease progressively as the number of openings increased (see Figure 31). The beam with a single opening (C100R) retained stiffness close to that of the reference solid-web specimen, with only a moderate reduction due to the localised removal of web material. The stiffness reduction became more pronounced in C100R2 and further in C100R3, where the elastic slope of the load–deflection curve was significantly diminished. The reduction in failure load was about 47.61% and 47.37% for C100R2 and C100R3, respectively. Furthermore, both beams showed an increase in deflection value of 35.98% when compared to reference beams with a single web opening. This reduction is attributed to the disruption of shear flow and the effective loss of moment of inertia as additional openings are introduced along the span.

The ultimate load capacity followed a clear descending trend:

□□(C100R)>□□(C100R2)>□□(C100R3). The single-opening beam sustained a relatively high ultimate load with acceptable ductility, whereas the two- and three-opening specimens exhibited marked reductions in capacity. In particular, the C100R3 specimen showed a sharper post-peak decline, reflecting a more brittle failure mode driven by local buckling of the reduced web panels and overstress of the adjacent shear studs.

Figure 31 shows the numerical load–displacement response for three composite beam specimens with rectangular web openings and a 70% shear stud connection ratio: C-70R (single opening), C-70R2 (two openings) and C-70R3 (three openings). The following observations and interpretations are drawn from the figure. C-70R exhibits a much steeper initial slope (highest elastic stiffness). C-70R2 and C-70R3 follow nearly identical, substantially lower initial slopes. The single-opening specimen (C-70R) attains roughly 2 × the load capacity of the multi-opening specimens (C-70R2/C-70R3). C-70R reaches a much higher load quickly and then gently approaches a plateau near ≈1100 kN. Both C-70R2 and C-70R3 reach an earlier plateau around ≈500‑550 kN. The black and red curves almost coincide throughout the loading history. Effect of increasing openings: Moving from one to two openings produces a large reduction in stiffness and strength; adding a third opening (C-70R3) produces very little further reduction—the two- and three-opening cases behave almost the same.

The initial stiffness of the C-70R specimen was considerably higher than that of the multi-opening specimens. This indicates that with partial shear connection, the presence of a single opening does not completely disrupt the overall composite action, and the beam retains a relatively high effective flexural rigidity. In contrast, C-70R2 and C-70R3 displayed almost identical and much lower initial slopes. This suggests that the introduction of a second opening reduces the continuity of shear transfer in the web to a critical level, after which additional openings do not substantially alter the global stiffness.

The load–deflection responses of beams with a 50% shear stud connection are presented in Figure X.X for specimens with one rectangular opening (C-50R), two openings (C-50R2), and three openings (C-50R3). The results reveal that both the degree of shear connection and the number of web openings play a critical role in governing the stiffness, strength, and ductility of composite beams. Specimen C-50R exhibited the highest initial stiffness among the three configurations, with a sharp linear rise in load up to approximately 900 kN. In contrast, both C-50R2 and C-50R3 showed much shallower initial slopes, reflecting a significant reduction in flexural rigidity due to the disruption of shear transfer in the web. The similarity in the slopes of C-50R2 and C-50R3 suggests that once two openings were introduced, the stiffness reduction reached a critical threshold, and additional openings did not further decrease the initial rigidity. The peak load of C-50R exceeded 1100 kN, more than double that of C-50R2 and C-50R3, which reached only about 500–550 kN. This highlights that, under a half shear connection, the presence of a single opening allows the beam to retain considerable strength, while two or more openings result in a drastic capacity reduction.

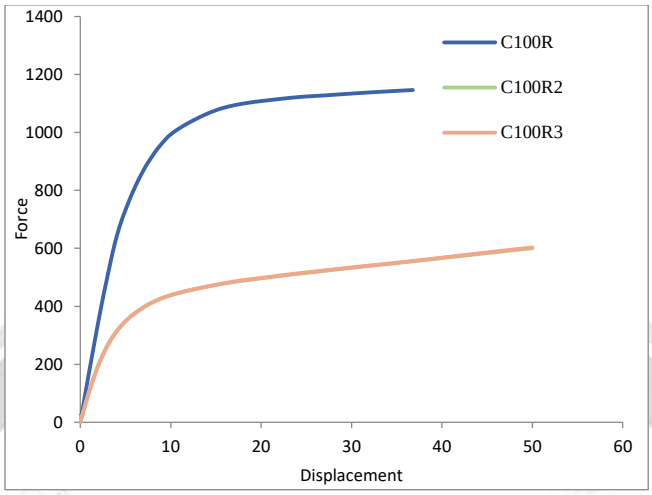

(a) 100% connections ratio

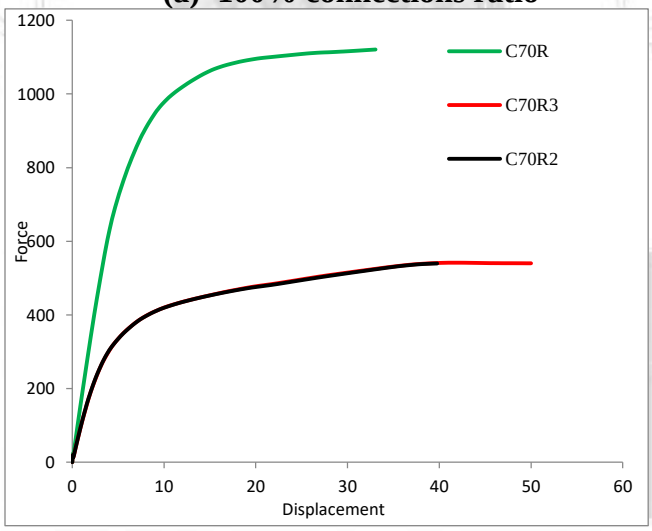

(b) 70% connections ratio

Table 11: The ultimate loads and deflection of the tested specimens with variety web opening.

Beam designation	Ultimate capacity (kN)	Failure load increase over Control beam *	max (mm)	Ratio relative to the control beam*	Failure mode
C-100R	1145.98	--	36.77	--	Shear failure
C-100R2	600.338	-47.61	50	+35.98	Shear failure
C-100R3	603.171	-47.37	50	+35.98	Shear failure
C-70R	1120.69	--	33.05	--	Shear failure

C-70R2	539.624	-51.85	39.78	+20.36	Shear failure
C-70R3	540.11	-51.81	50	+51.29	Shear failure
C-50R	1113.27	--	44.06	--	Shear failure
C-50R2	540.804	-51.42	50	0.00	Shear failure
C-50R3	537.075	-51.76	50	0.00	Shear failure
C-100RY	1138.93	--	50	--	Shear failure
C-100R2Y	576.775	-49.36	50	0.00	Shear failure
C-100R3Y	575.058	-49.51	50	0.00	Shear failure
C-70RY	1123.94	--	50	--	Shear failure
C-70R2Y	555.308	-50.59	50	0.00	Shear failure
C-70R3Y	554.698	-50.65	50	0.00	Shear failure
C-50RY	1102.37	--	50	--	Shear failure
C-50R2Y	525.56	-52.32	50	0.00	Shear failure
C-50R3Y	525.373	-52.34	50	0.00	Shear failure

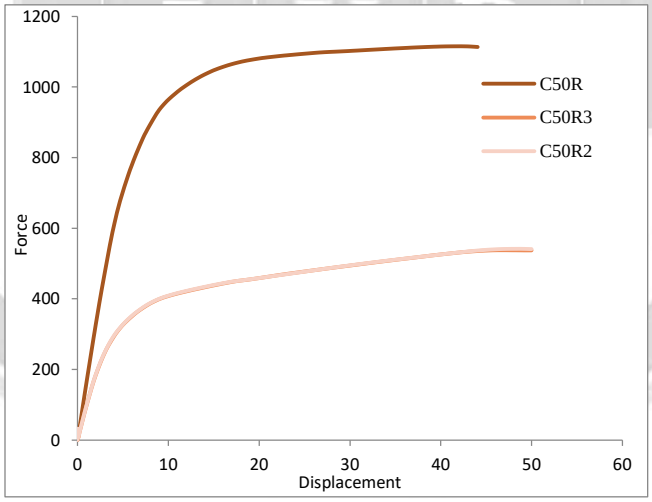

(c) 50% connections ratio

Fig. 31. Load–deflection response for the tested composite beams made with a rectangular web opening reinforced with shear studs connections.

The numerical load–deflection curves for beams with Y-rib shear connectors at a full connection ratio (100%) are illustrated in Figure 32. Three configurations were investigated: a single rectangular web opening (C100RY), two openings (C100R2Y), and three openings (C100R3Y). The results clearly demonstrate the influence of multiple web openings on the stiffness, strength, and ductility of fully connected composite beams.

The specimen with a single opening (C100RY) showed the steepest initial slope, reflecting the highest flexural stiffness among the three beams. The incorporation of two (C100R2Y) and three openings (C100R3Y) reduced the initial stiffness considerably, as evident from the flatter rise in the early load–deflection stages. This reduction is primarily due to the discontinuity in the web, which disrupts shear flow and reduces the overall rigidity of the section, even though the shear connection ratio was maintained at 100%.C100RY achieved the maximum strength of approximately 1150 kN, while C100R2Y and C100R3Y reached only about 550–570 kN. This corresponds to a reduction of nearly 52–54% in load-bearing capacity when moving from a single opening to two or three openings. In other words, C100RY carried more than twice the load of C100R2Y and C100R3Y. The close similarity between C100R2Y and C100R3Y highlights that the critical weakening mechanism is already triggered once two openings are present, and the third opening does not proportionally reduce the capacity further. At ultimate load, C100RY sustained displacements of around 45–50 mm, whereas C100R2Y and C100R3Y showed similar displacement ranges of about 48–50 mm. This indicates that while ultimate load dropped significantly with more openings, the beams with two and three openings still achieved comparable deformation levels. Relative to C100RY, C100R2Y and C100R3Y exhibited about a 10% higher deflection capacity at failure, but with less than half the load resistance, reflecting reduced stiffness and energy absorption efficiency.

Figure 32 presents the experimental load–deflection curves for web rectangular composite beams with 70% Y-rib connections, designated as C-70RY, C-70R2Y, and C-70R3Y. The results demonstrate a clear variation in behavior among the three connection types:

C-70RY exhibited the highest load capacity and stiffness, with a steep initial slope in the load–deflection curve. This reflects effective shear transfer between the steel and concrete components, producing near-full composite action. The load carried at midspan deflections beyond 30 mm remained above 1,000 kN, indicating excellent serviceability performance.

C-70R2Y and C-70R3Y showed noticeably lower stiffness and ultimate load capacity, reaching only about 45–50% of the peak load sustained by C-70RY. Both specimens followed a very similar response throughout the loading regime, suggesting that additional rib layers beyond the second did not significantly improve stiffness or capacity when only 70% of the rib depth was engaged. This may be attributed to slip along the interface or premature local yielding that limited the effective participation of deeper ribs.

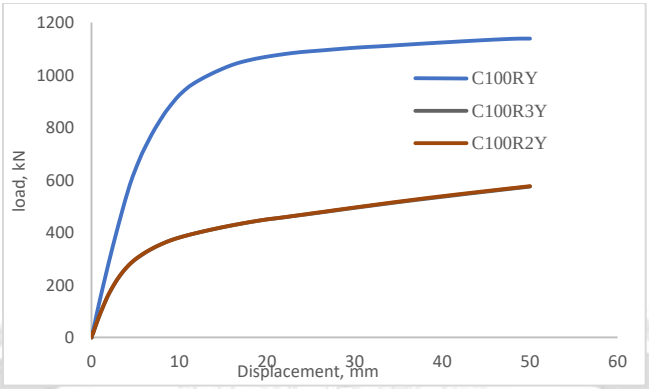

(a) 100% connections ratio

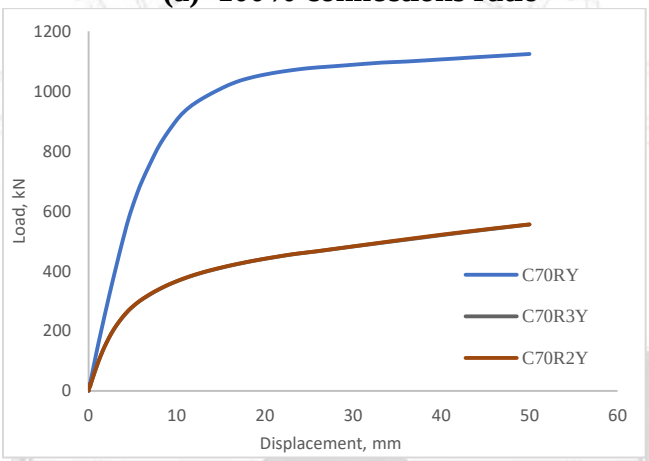

(b) 70% connections ratio

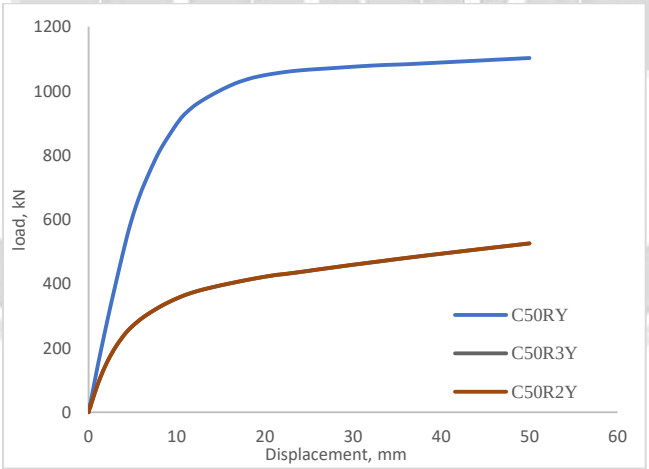

(c) 50% connections ratio

Fig. 32. Load–deflection response for the tested composite beams made with a rectangular web opening reinforced with Y-rib shear connections.

2) Crack Patterns and Failure Modes

Figure 33 shows the crack propagation and failure modes of composite beams reinforced with shear studs for three groups of rib engagement (C100, C70, and C50). Within each group, the effect of increasing the number of openings (single, two, and three) is compared.

C100 Group (C100R, C100R2, C100R3):

In the 100% rib connection group, the specimen with a single opening (C100R) displayed the most stable behavior, with cracks concentrated at the corners of the opening and propagating diagonally into the web. When two openings were introduced (C100R2), crack intensity increased around both openings, especially in the central web between them, where stress concentrations were evident. With three openings (C100R3), cracks became more widespread and linked across the web depth, showing a clear reduction in stiffness. Nevertheless, due to the high rib engagement and stud reinforcement, the C100 series retained better crack control and higher ductility compared to the other groups.

C70 Group (C70R, C70R2, C70R3):

In the 70% rib connection group, the single-opening specimen (C70R) exhibited controlled cracking similar to C100R, but with slightly wider crack development. Adding two openings (C70R2) caused significant crack propagation around both openings and increased stress demand in the web region between them, resulting in earlier stiffness degradation. With three openings (C70R3), the cracks became severe and extended across the depth, merging into continuous failure paths. Compared to the C100 series, the C70 group demonstrated reduced crack resistance, although the studs still delayed premature slip and maintained a progressive failure mode.

C50 Group (C50R, C50R2, C50R3):

The 50% rib connection group showed the most critical crack development. The single-opening specimen (C50R) already exhibited wide diagonal cracks around the opening corners, indicating higher stress concentration. With two openings (C50R2), the cracks widened further and extended into the mid-web, producing early stiffness loss. The three-opening specimen (C50R3) displayed the most severe behavior, with multiple diagonal cracks merging into continuous web failures, reflecting a brittle shear-dominated mode. Despite shear stud reinforcement, the C50 group retained the least structural capacity and weakest crack control among all groups.

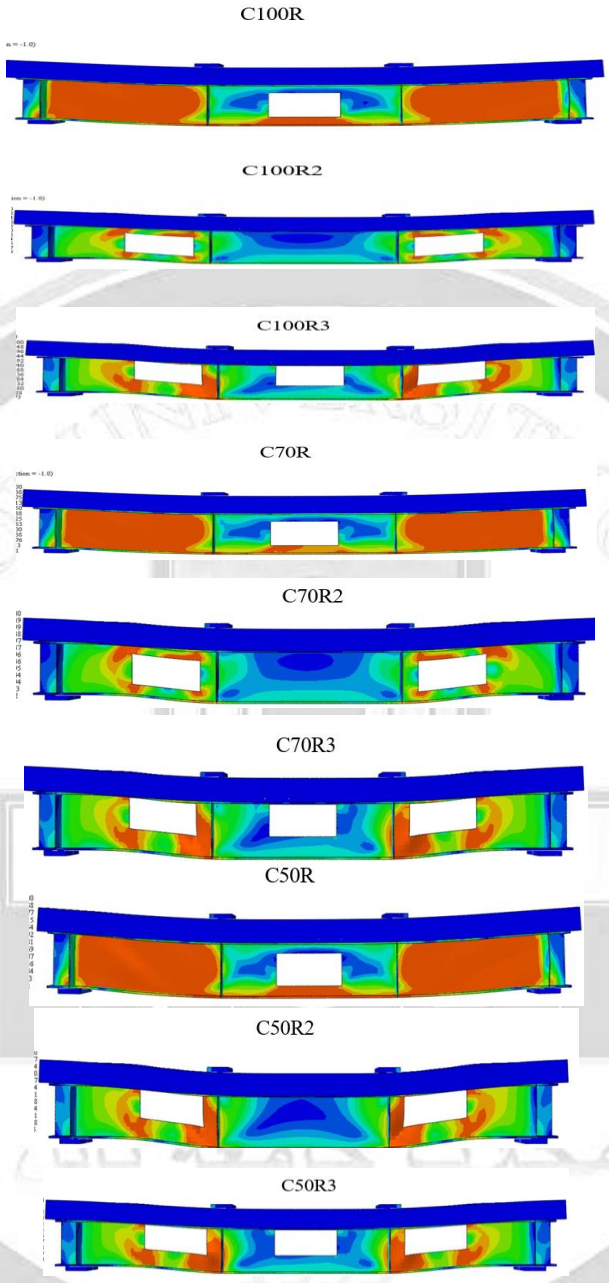

Fig. 33. Crack pattern and failure mode for opening composite beams reinforced shear studsconnection.

The crack distribution for composite beams with different web opening configurations and varying connection ratios (100%, 70%, and 50%) is illustrated in Figure 34. Each group of beams (C100, C70, and C50) is discussed individually to highlight the influence of the number of openings and the connection ratio on crack propagation mechanisms.

1. C100 Group (C100R, C100R2, C100R3)

The beams in the C100 group were designed with a 100% connection ratio, which provided the highest degree of composite action between the steel and concrete.

C100R (Single Opening): Cracks were mainly localized around the perimeter of the web opening, with diagonal patterns forming at the corners. The Y-rib reinforcement effectively confined the stresses, delaying their spread into the web and flanges.

C100R2 (Double Openings): The presence of two adjacent openings introduced stress interaction in the intermediate web panel. Cracking was more extensive, with diagonal cracks linking both openings, resulting in a wider cracked region compared to C100R.

C100R3 (Triple Openings): The crack propagation became continuous along the central span, extending across all three openings. Despite the Y-ribs, the stress redistribution between openings created significant diagonal and shear cracks into the flanges.

Thus, For C100 beams, the increase in the number of openings directly increased crack severity. While Y-ribs effectively controlled localized corner stresses, the triple-opening specimen (C100R3) showed the most critical cracked region due to interaction between multiple openings.

2. C70 Group (C70R, C70R2, C70R3)

The beams in the C70 group had a 70% connection ratio, reducing the composite action compared to the C100 series. This lower degree of shear transfer made the beams more sensitive to cracking.

C70R (Single Opening): Crack patterns were similar to C100R but more pronounced in size and intensity due to weaker composite action. Diagonal cracks at the corners of the opening extended further into the web region.

C70R2 (Double Openings): The intermediate web panel experienced severe stress concentration, leading to stronger crack connectivity between the two openings compared to C100R2.

C70R3 (Triple Openings): The triple-opening beam exhibited widespread cracking, with cracks spanning across the central span and extending into both tension and compression flanges. The reduced connection ratio aggravated stress transfer inefficiency, making the cracked zones denser and more critical compared to the C100R3 specimen.

Therefore, For the C70 group, cracks developed earlier and propagated more aggressively than in the C100 group. The reduced composite action led to larger cracked zones even for the single-opening beam, and this effect became significantly worse for multiple openings.

3. C50 Group (C50R, C50R2, C50R3)

The C50 group, with a 50% connection ratio, represented the lowest level of composite interaction among all groups. This significantly influenced crack development and spread.

C50R (Single Opening): Cracks around the opening corners propagated more widely than in the C70R and C100R specimens. Stress redistribution was less controlled, resulting in earlier crack initiation.

C50R2 (Double Openings): The intermediate web panel between openings became a critical failure zone, showing rapid development of interconnected diagonal cracks.

C50R3 (Triple Openings): The crack distribution was the most severe among all tested specimens. The reduced composite action, combined with the presence of three openings, created an almost fully cracked central span, with shear cracks extending into both flanges and the web.

The results present that The C50 group showed the weakest crack resistance. As the number of openings increased, the severity of cracking intensified dramatically, confirming that reduced connection ratio combined with multiple openings accelerates crack growth and reduces beam integrity.

When compared with all groups, C100 Group: showed the most controlled crack patterns, with Y-rib reinforcement effectively managing local stresses. However, multiple openings still reduced performance. C70 Group: Cracks were more severe than in C100 beams, with larger spread due to reduced composite action. C50 Group: Exhibited the earliest and most extensive cracking, especially in triple-opening beams, confirming that both the number of openings and reduced connection ratio critically affect crack propagation.

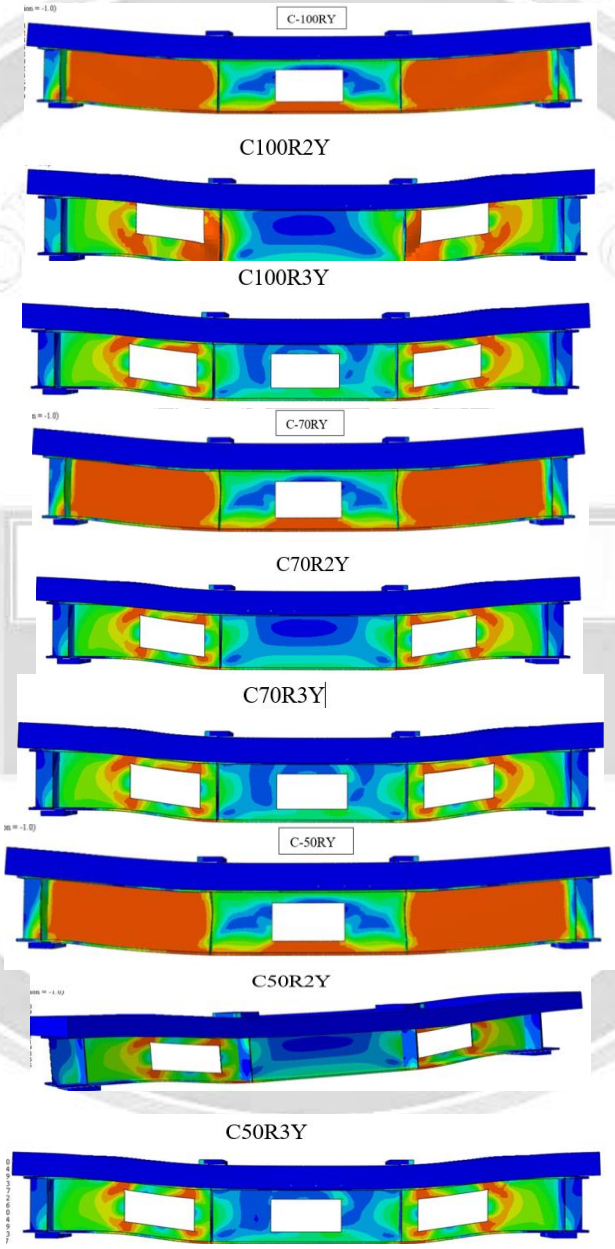

Fig. 34. Crack pattern and failure mode for opening composite beams reinforced Y-rib connection.

V. Conclusions

A numerical investigation into the response of a composite concrete beam encasing steel girder under static loads was presented. For this purpose, twelve specimens made with different types of shear connectors were considered. Two variables were considered in the numerical tests, including the types of shear connectors and the web opening. The following conclusion can be drawn from the present study:

1. The test results indicate that all composite beam specimens primarily exhibited shear failure as the dominant failure mode.
2. Rectangular web openings not only enhance the shear deformation of composite beams but also produce a redistribution of internal forces.
3. The presence of web openings affects the bearing capacity and deformation capacity, while decreasing the stiffness and strength of composite steel-concrete beams.
4. The calculated percentage increases in the maximum stress area of the steel beam are 25%, and 72% for the beam with rectangular, and circular openings, respectively, in comparison to the beam without an opening. There is an increase observed in deflection of 14%, and 47% for the rectangular, and circular opening composite beam, respectively, compared to the beam without opening.
5. Circular web openings have been discovered to be very effective in all aspects, including low stress concentration at the web openings and ease of fabrication relevantly.
6. Web opening affects the composite steel-concrete beams and decreases the stiffness and strength of simply supported composite steel-concrete beams.
7. The strain distribution at the web opening of prefabricated composite beams no longer conforms to the plane hypothesis but presents an “S” distribution.

References

[1] Shamass, R., and Cashell, K. A., “Behaviour of composite beams made using high strength steel,” Structures, Vol. 12, 2017, pp. 88–101.

[2] Mansour, F. R., Bakar, S. A., Ibrahim, I. S., Marsono, A. K., and Marabi, B., “Flexural performance of a precast concrete slab with steel fiber concrete topping,” Construction and Building Materials, vol.75, 2015, pp.112–120.

[3] Khadhair A. Y., and Izzet A. F., “Behavior of Reinforced Concrete Beams with Vertically Penetrated Holes across the Cross-section Deoth,” Engineering, Technology & Applied Science Research, vol. 14, No. 3, 2024, pp.14301-14307.

[4] Ali D. Y., and Mahmood R. A., “Influence of Slenderness Ratio and Section Geometry on the Behavior of Steel Braced Frames,” Engineering, Technology & Applied Science Research, vol. 14, No. 3, 2024, pp.14282-14286.

[5] Ali S. N. H. Ramli Sulong M. S., and M. S., "Investigation of channel shear connectors for composite concrete and steel T-beam, "International Journal of the Physical Sciences, vol. 7, No.11, 2012. https://doi.org/10.5897/ijps11.1604.

[6] Ollgaard J.G., Slutter R.G., and Fisher J.W., "Shear strength of stud connectors in lightweight and normal-weight concrete," J. ACI Struct., 1971;8:55–64.

[7] Oehlers D.J., and Coughlan C.G., "The shear stiffness of stud shear connections in composite beams," J. Constr. Steel Res., 1986; 6:273–84.

[8] Shim C.S., Lee P.G., and Yoon T.Y., "Static behaviour of large stud shear connectors. Eng. Struct., 2004;26:1853–60.

[9] Mirza O., and Uy B.," Behavior of headed stud shear connectors for composite steel concrete beams at elevated temperatures," J. Constr. Steel Res., 2009;65:662–74.

[10] Mirza O., Uy B.," Effects of strain regimes on the behaviour of headed stud shear connectors for composite steel–concrete beams," Adv. Steel Constr., 2010;6 (1):635–61.

[11] Marshall W.T., Nelson H.M., and Banerjee H.K.," An experimental study of the use of high-strength friction grip bolts as shear connectors in composite beams," Struct. Eng., 49(4), PP. 171–178, 1971.

[12] Kwon G., Engelhardt M.D., and Klingner R.E.," Behavior of post installed shear connectors under static and fatigue loading," J. Constr. Steel Res., 66(4), PP.532–541, 2010a.

[13] Kwon G., Engelhardt M.D., and Klingner R.E," Experimental behavior of bridge beams retrofitted with post installed shear connectors," J. Bridge Eng., 16(4), PP.536–545, 2010b.

[14] Moynihan M.C., and Allwood J.M., "Viability and performance of demountable composite connectors," J. Constr. Steel Res., 99, PP.47–56, 2014.

[15] Mirza O., Uy B., and Patel N., "Behavior and strength of shear connectors utilising blind bolting," Paper presented to the 4th International Conference on Steel and Composite Structures: Sydney, PP. 21–23 July 2010.

[16] Moynihan M.C., and Allwood J.M., "Viability and performance of demountable composite connectors," J. Constr. Steel Res., 99, PP.47–56, 2014.

[17] Mirza O., Uy B., and Patel N., "Behavior and strength of shear connectors utilising blind bolting," Paper presented to the 4th International Conference on Steel and Composite Structures: Sydney, PP. 21–23 July 2010.

[18] Thevendran V., Shanmugam N. E., Chen S., and Liew J. Y. R., "Experimental study on steel concrete composite beams curved in plan," Eng. Struct., vol. 22, no. 8, pp. 877–889, Jun. 2000, https://doi: 10.1016/S0141-0296(99)00046-2.

[19] P. Rajaram, A. Murugesan, and G. S. Thirugnanam, "Experimental Study on Behavior of Interior RC Beam Column Joints Subjected to Cyclic Loading", (International Journal of Applied Engineering Research, Din Digul, Vol.1, No.1, 2010), pp. 49-59.

[20] O. C. Zienkiewicz, and R. L. Taylor, "The finite element method," Volume, vol. 1, pp.1992, 128–132.

[21] Clawson, W.C., Darwin, D. (1982). Tests of composite beams with web openings. Journal of the Structural Division, 108(1): 145-162. https://doi.org/10.1061/JSDEAG.0005856

[22] Donahey, R.C., Darwin, D. (1988). Web openings in composite beams with ribbed slabs. Journal of Structural Engineering, 114(3): 518-534. https://doi.org/10.1061/(ASCE)0733-9445(1988)114:3(518)

[23] Redwood, R.G., Poumbouras, G. (1983). Tests of composite beams with web holes. Canadian Journal of Civil Engineering, 10(4): 713-721. https://doi.org/10.1139/l83-100

[24] Fahmy, E.H. (1996). Analysis of composite beams with rectangular web openings. Journal of Constructional Steel Research, 37(1): 47-62. https://doi.org/10.1016/0143-974X(95)00022-N

[25] Benitez, M.A., Darwin, D., Donahey, R.C. (1998). Deflections of composite beams with web openings. Journal of Structural Engineering, 124(10): 1139-1147. ttps://doi.org/10.1061/(ASCE)07339445(1998)124:10(1139)

[26] Park, J.W., Kim, C.H., Yang, S.C. (2003). Ultimate strength of ribbed slab composite beams with web openings. Journal of Structural Engineering, 129(6): 810-817. https://doi.org/10.1061/(ASCE)0733-9445(2003)129:6(810)

[27] Al-Rekabi, A.H., Abo Dhaheer, M.S. (2024). Flexural performance of sustainable hybrid fibre-reinforced SCC beams made of treated recycled aggregates. Journal of Building Pathology and Rehabilitation, 9(1): 33. https://doi.org/10.1007/s41024-023-00382-3

[28] Al-Rekabi, A.H., Al-Marmadi, S.M., Dhaheer, M.A., Al-Ramahee, M. (2023). Experimental investigation on sustainable fiber reinforced self-compacting concrete made with treated recycled aggregate. AIP Conference Proceedings, 2775(1): 020032. https://doi.org/10.1063/5.0140655

[29] Hagen, N.C., Larsen, P.K., Aalberg, A. (2009). Shear capacity of steel plate girders with large web openings, Part I: Modeling and simulations. Journal of Constructional Steel Research, 65(1): 142-150. https://doi.org/10.1016/j.jcsr.2008.03.014

[30] Hagen, N.C., Larsen, P.K. (2009). Shear capacity of steel plate girders with large web openings, Part II: Design guidelines. Journal of Constructional Steel Research, 65(1): 151-158. https://doi.org/10.1016/j.jcsr.2008.03.005

[31] Sheehan, T., Dai, X., Lam, D., Aggelopoulos, E., Lawson, M., Obiala, R. (2016). Experimental study on long spanning composite cellular beam under flexure and shear. Journal of constructional steel research, 116: 40-54. https://doi.org/10.1016/j.jcsr.2015.08.047

[32] Ellobody, E., Young, B. (2015). Behaviour and design of composite beams with stiffened and unstiffened web openings. Advances in Structural Engineering, 18(6): 893-918. https://doi.org/10.1260/1369-4332.18.6.893

[33] Lawson, R.M., Chung, K.F., Price, A.M. (1992). Tests on composite beams with large web openings to justify existing design methods. Structural Engineer London, 70(1): 1-7.

[34] Yazıcı, H., Yiğiter, H., Aydın, S., Baradan, B. (2006). Autoclaved SIFCON with high volume class C fly ash binder phase. Cement and concrete research, 36(3): 481-486. https://doi.org/10.1016/j.cemconres.2005.10.002

[35] Liao, W., Li, L., Liu, D., Dai, B., Wang, C. (2018). Nonlinear FEM analysis on composite beams with web opening under negative bending moment. Tehnički Vjesnik, 25(5): 1546-1552. https://doi.org/10.17559/TV-20180626222438

[36] Li, L., Liao, W., Wang, J., Zhou, D. (2015). Behavior of continuous steel-concrete composite beams with web openings. International Journal of Steel Structures, 15(4): 989-997. https://doi.org/10.1007/s13296-015-1218-2

[37] Ellobody, E., Al-Salloum, Y., & Tounsi, A. (2012). Finite element analysis of composite beams with stiffened and unstiffened web openings. Engineering Structures, 41, 45–55. https://doi.org/10.1016/j.engstruct.2012.03.010

[38] Hu, X., Zhang, Y., & Li, W. (2018). Flexural performance of composite beams with stiffened web openings under three-point bending. *Journal of Constructional Steel Research*, *148*(2), 45–57. https://doi.org/10.1016/j.jcsr.2018.05.004

[39] Mastan, M., Khan, R., & Ali, S. (2020). Numerical study of composite steel–concrete beams with different web opening shapes using ABAQUS. *Journal of Constructional Steel Research, 170*, 106045. https://doi.org/10.1016/j.jcsr.2020.106045

[40] Li, L., Zhang, H., Zhou, D. (2021). Experimental study of high-strength bolt connected composite beams with web openings. Iranian Journal of Science and Technology, Transactions of Civil Engineering, 45(1): 1-10. https://doi.org/10.1007/s40996-020-00411-y

[41] R. Malm, “Shear cracks in concrete structures subjected to in-plane stresses.” KTH, 2006.

[42] Eriksson, D., Gasch, T. (2010). FEM-modeling of reinforced concrete and verification of the concrete material models available in ABAQUS. Royal Institute of Technology, Stockholm, SWEDEN.

[43] DR. T. S. Babu, and M. P. Kumar. ,"A Study on Shear Strength of Steel Fiber Reinforced Concrete.", (2017, 06(14), pp.2769–2778.

[44] Rajaram, P., Murugesan, A., Thirugnanam, G.S. (2010). Experimental Study on behavior of interior RC beam column joints subjected to cyclic loading. International journal of applied engineering research, Dindigul, 1(1): 49-59.

[45] Thevendran, V., Shanmugam, N.E., Chen, S., Liew, J.R. (2000). Experimental study on steel-concrete composite beams curved in plan. Engineering Structures, 22(8): 877-889. https://doi.org/10.1016/S0141-0296(99)00046-2

[46] Sika Corporation, Product Data Sheet for “Sika Wrap®-300”, 34957 Tuzla, İstanbul, Türkiye, (www.sika.com).

[47] Afazov, S.M., Becker, A.A., Hyde, T.H. (2012). Mathematical modeling and implementation of residual stress mapping from microscale to macroscale finite element models. Journal of Manufacturing Science and Engineering, 134(2): 021001. https://doi.org/10.1115/1.4006090

[48] Hibbitt, Karlsson & Sorensen Inc. (2011). ABAQUS Analysis User's Manual, Version 6.11. Providence, RI: Dassault Systèmes Simulia Corp.

[49] Malm, R. (2009). Shear cracks in concrete structures subjected to in-plane stresses (Doctoral dissertation, Royal Institute of Technology, KTH). Stockholm, Sweden: KTH Architecture and the Built Environment.

[50] Sarsam, K.F., Mohammed, M.H. (2014). Load-deflection behavior of hybrid beams containing reactive powder concrete and conventional concrete. Journal of Engineering and Sustainable Development, 18(3): 118-147.

[51] Vijayakumar, M., Kumar, P.D. (2017). Study on strength properties of SIFCON. International Research Journal of Engineering and Technology (IRJET), 4(1): 235-238.

[52] Saenz, L. P. (1964). Discussion of "Equation for the stress-strain curve of concrete" by Desayi and Krishnan. Journal of the American Concrete Institute, 61(9), 1229–1235.

[53] Hibbitt, Karlsson & Sorensen Inc. (2011). ABAQUS Analysis User's Manual, Version 6.11. Providence, RI: Dassault Systèmes Simulia Corp.

[54] Massicotte, B., Mohammadi, S., & Mirza, F. A. (1990). Tension-stiffening model for reinforced concrete elements. Journal of Structural Engineering, 116(1), 242–259. https://doi.org/10.1061/(ASCE)0733-9445(1990)116:1(242)

ARTICLE
JOURNAL`S UNIVERSITY OF BABYLON FOR ENGINEERING SCIENCES (JUBES)
مـــجلـة جـــامعة بـــابـل للعلـــوم الهندسية
Vol. 34, No. 1. \ 2026 ISSN: 2616 - 9916

دراسة عددية للعوارض المركبة ذات الفتحات المستطيلة والدائرية المصنوعة باستخدام موصلات القص المتنوعة

علي حبيب نوري عبد الناصر محمد الجعفر

قسم الهندسة المدنية، كلية الهندسة، جامعة البصرة ،العراق، البصرة

pgs.ali.habeeb@uobasrah.edu.iq

الخلاصة

قدم البحث الحالي تقييمًا عدديًا لسلوك عوارض الفتح المركبة المبنية بوصلات قص مختلفة تحت ظروف تحميل من أربع نقاط. تم تحليل سلسلة من عوارض الفولاذ والخرسانة المركبة ذات أشكال فتح مختلفة وأعداد فتحات وأنواع مختلفة من وصلات القص رقميًا. تم فحص أربعة متغيرات: نسب التوصيل 100٪ و 70٪ و 50٪ ؛ أنواع موصلات القص) المسامير ووصلات (Y–rib ؛ أشكال فتحات الويب (مستطيلة ودائرية) ؛ وعدد الفتحات. تضمنت استنتاجات الدراسة انحراف العارضة في منتصف الامتداد وحمل التشقق ونمط التشقق ووضع الفشل. تشير هذه النتائج إلى أن وصلات قص Y–rib هي الأفضل من بين جميع الموصلات المستخدمة. لقد عززت سعة القص القصوى بنحو 1.88٪ و 2.28٪ و 3.21٪ لنسب التوصيل 50٪ و 70٪ و 100٪ على التوالي. علاوة على ذلك، يُقلل دمج فتحات النسيج من صلابة ومتانة عوارض الفولاذ والخرسانة المركبة، مع زيادة قدرتها على التحمل والتشوه. يؤثر هذا الدمج على عوارض الفولاذ والخرسانة المركبة، ويُقلل من صلابة ومتانة عوارض الفولاذ والخرسانة المركبة ذات الدعامات البسيطة. من ناحية أخرى، ثَبُتَ أن فتحات النسيج الدائرية تُؤدي وظيفتها بكفاءة في جميع الجوانب، بما في ذلك الحفاظ على انخفاض الإجهاد عند فتحات النسيج، وتسهيل بنائها. مع ذلك، كان فشل القص أكثر أنواع الفشل شيوعًا في جميع عينات العوارض المركبة.

الكلمات الدالة: العوارض المركبة، فتحة الدائرة، موصل الضلع Y، وضع الفشل، السلوك الهيكلي.